IEEE Access
Multidisciplinary ⋮ Rapid Review ⋮ Open Access Journal

Received March 23, 2022, accepted April 23, 2022, date of publication April 28, 2022, date of current version May 6, 2022.

Digital Object Identifier 10.1109/ACCESS.2022.3170912

Literature Review: On-Chip Photonic Crystals and Photonic Crystal Fiber for Biosensing and Some Novel Trends

NAZMI A. MOHAMMED[1], OMAR E. KHEDR[2], EL-SAYED M. EL-RABAIE[3], AND ASHRAF A. M. KHALAF[4]

[1]Photonic Research Laboratory, Electrical Engineering Department, College of Engineering, Shaqra University, Shaqra, Riyadh 11961, Saudi Arabia
[2]Department of Communications and Electronics, Alexandria Higher Institute for Engineering and Technology, Alexandria Governorate 21311, Egypt
[3]Department of Electronics and Communications Engineering, Faculty of Electronic Engineering, Menoufia University, Menouf 32952, Egypt
[4]Department of Communications and Electronics, Faculty of Engineering, Minia University, Minia 61111, Egypt

Corresponding author: Omar E. Khedr (omar_7525@hotmail.com)

ABSTRACT This review summarizes recent advances in sensors based on photonic crystal technologies for biomedical sensing applications. Photonic crystal sensing offers enormous promise due to their clear benefits in sensitivity, stability, compactness, portability. This work discusses several photonic crystal structures, such as photonic crystal waveguides, cavities, and photonic crystal fiber for biomedical sensing applications. The uniqueness, measurement technique, and biosensing properties of each type of these structures are discussed. Furthermore, manufacturing and functionally relevant properties that include design simplicity, compactness, and multi-wavelength operation are also reviewed. They are explored, organized, and compared using the most recent related literature in this field. Finally, a brief of novel trends has been introduced.

INDEX TERMS Biomedical sensors, photonic crystals, photonic crystal fiber.

I. INTRODUCTION

For the last couple of decades, tremendous research has been conducted in the development of inexpensive, accurate, and reliable biomedical sensors capable of measuring extremely low concentrations of analytes. Numerous sensors have been created and manufactured to control and detect gases, fluids, and cells using several technologies.

Among these technologies, photonic crystals (PhC) have become more popular due to their promising characteristics such as their ultra-compact size, minimal analyte requirement, excellent measurement sensitivity, flexibility in structural design, and integration capability [1], [2]. Additionally, PhC can inherit excellent optical features, such as safety in a flammable, explosive environment, immunity to electromagnetic interference, long-range monitoring, and rapid response speed [3], [4]. Previous merits makes PhC one of the most attractive optical data processing platforms. These platforms contain famous photonic based technologies as: semiconductor optical amplifiers (SOAs) [5], Mach–Zehnder interferometer (MZI) [6], [7], fiber Bragg grating (FBG) [8]–[10], free-space optical communication (FSO) [11], [12], visible light communications (VLC) [13]–[19], and modulators used in optical networks [20]. Recently, PhC are widely used in several optical data processing applications as: a resonator [21], [22], coupler [23], channel drop filters [24], [25], optical modulators [26], oscillators [27], switches [28], logic gates [29]–[31], adders [32], [33], subtractors [34], [35], encoders [36], and sensors.

PhC-based sensors are among the most promising sensing technologies of today. Their unique physical characteristics, such as reflectance/transmittance, enabled outstanding sensitivity levels, resulting in precise detection limits are obtained. Because of their gleaming visual quality, a suitable display in the visible range of wavelengths is an additional advantage. High sensing selectivity and superior light confinement in minimal quantities are further benefits [37], [38]. Many types of PhC based sensors are high-temperature sensors [39], [40], gas [41], biomedical [42]–[44], displacement [45], [46], liquid [47], [48] and force-strain sensors [49]–[52].

Nanoscale light manipulation has the potential to enable a variety of technological improvements in PhC biomedical sensing. Numerous ways have been devised to achieve compactness, simplicity, excellent quality, and sensitivity. These are the primary criteria for determining the reliability of biomedical sensor assessment parameters [43], [53].

The associate editor coordinating the review of this manuscript and approving it for publication was Sukhdev Roy.

An intensive review of biomedical sensors based on photonic crystal fiber and on-chip photonic crystals has been presented through this work. An exploration is provided about the operating techniques and essential performance evaluation parameters (i.e., evaluation metrics). A concise elaboration is provided, followed by a comparison table between various types of PhC biomedical sensors. The evaluation metrics have been discussed. Future trends that are required to realize next-generation PhC biomedical sensors are also highlighted. The remaining of this article is organized as follows: The photonic crystal platforms and evaluation metrics for biomedical sensing exist in part II. In part III, A survey on on-chip photonic crystal biomedical sensors is presented. The review on famous literatures for photonic crystal fiber biomedical sensors is presented in part IV. Numerical methods and the allowable commercial software packages that are used for designing, testing, and evaluating such sensors are reviewed in part V. Some novel trends that are related to the PhC based biomedical sensors are presented in part VI. Finally, the conclusion is drawn in part VII.

II. PHOTONIC CRYSTAL PLATFORMS AND EVALUATION METRICS FOR BIOMEDICAL SENSING

A. ON-CHIP PHOTONIC CRYSTAL

Photonic crystal on-chip sensors depend mainly on a cavities deformation of the structure. PhCs cavities are one of the most powerful advantages of photonic crystals. The cavity of PhCs can form by removing one pillar or filling one hole. Point defects can control light in cavities. PhC cavities have different shapes, such as single or double, or triple cavities, as shown in Figure 1 [54]. Cavities are the most frequent type of PhC configuration. They consist of a 2D periodic PhC slab with an etched triangle or square lattice of air holes. Light is navigable by the periodic structure inside the planes in the 2D PhC [55]. However, total internal reflection gives confinement in the third dimension. By creating defects inside the arranged structures of the refractive index, such as eliminating holes or ever-changing radii, confinement will be accomplished [56]. As a result, accessible states for a narrowband portion of radiation within the bandgap are created, preventing propagating of waves in these areas [57], [58].

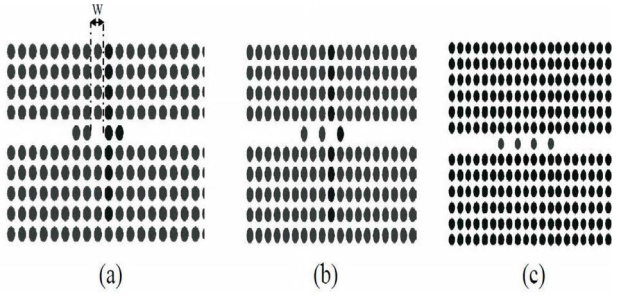

FIGURE 1. Photonic crystal with (a) Single cavity, (b) Double cavities, (c)Triple cavities.

On-chip Photonic crystal performance evaluation parameters (i.e., evaluation metrics) are the key to evaluating the performance of the sensor. For biomedical sensing applications quality factor (Q), compactness, and sensitivity (S), are considered as characteristic parameters. A multitude of parameters determines the biomedical sensor's effectiveness. The quality factor Q is a parameter that indicates how much energy is lost in a resonant cavity. A cavity can be formed by removing one pillar or filling one hole of a photonic crystal structure. If the quality factor is high, the loss of power is lower. The quality factor is defined as the ratio of the wavelength achieved at resonance λ to the wavelength variation at the Full-Width Half Maximum (FWHM) $\Delta\lambda$. The quality factor is being used to control the light in the cavity and reduce the loss of power. Quality should be as high as possible yet remain unitless [4], [59].

$$Q = \frac{\lambda_0}{\Delta\lambda_{FWHM}} \tag{1}$$

where λ_0 (resonant) is the wavelength at resonance and $\Delta\lambda_{FWHM}$ is the wavelength change at FWHM.

Sensitivity (S) is one of the most remarkable evaluation metrics of the sensors. It represents the ratio of the change in resonant wavelength due to refractive index variation to the measured change in refractive index variation. Sensitivity is expressed in nanometres per refractive index unit nm/RIU and should be as large as possible. The sensitivity of a sensor reveals how much its output varies in response to a bit of change in the input [4], [59].

$$S = \frac{\Delta\lambda}{\Delta n} \tag{2}$$

where $\Delta\lambda$ represents the change in resonant wavelength between the target sensing analyte and the normal case or air as a reference, and Δn represents the change in the refractive index between the target sensing analyte and normal case or air as a reference.

Finally, the size of the on-chip photonic crystal is one of the most effective evaluation metrics. It should be as compact as possible. The ideal design topology for a photonic crystal as a sensor is one of the most active research fields. This field of study has been studied for decades. The research is still ongoing since there are an infinite number of undiscovered topologies. One significant advantage of different design topologies is the ability to be fabricated by today's technology. However, certain topologies have difficult manufacturing process limits, such as a high fabrication cost, particularly in comparison to ordinary optical devices, and require the use of advanced fabrication techniques [51].

B. PHOTONIC CRYSTAL FIBER

Photonic crystal fibers (PCF) are one of the popular platforms for PhC. The propagation of light can be divided through PCF in two ways: The total internal reflection in which high index in the core that surrounded by an array of air holes, and the photonic bandgap (PBG) fiber emerging in which a lower index in the core or a hollow core. Figure 2 presents different views of the cross-section for PCF structures such

as solid-core, hollow-core, solid-core, holes filled with liquid and cylindrical hollow [60], [61].

PCF is used in various applications, including biomedical, chemical, and gas sensors. In recent years, many PCFs have been utilized widely in sensing due to their ability and superiority. Most PCFs use silica, TOPAS, and Zionex as background materials. Also, it is worth mentioning that most of the PCFs work in the frequency of the Terahertz region. The THz waves consider one of the photonic crystal applications in optical areas. Historically, technologically THz range was limited by the difficulty of generating and detecting. THz uses emitters, detectors, semiconductors, medical, manufacturing, space and biomedical imaging, defence industries such as security in military communications [62].

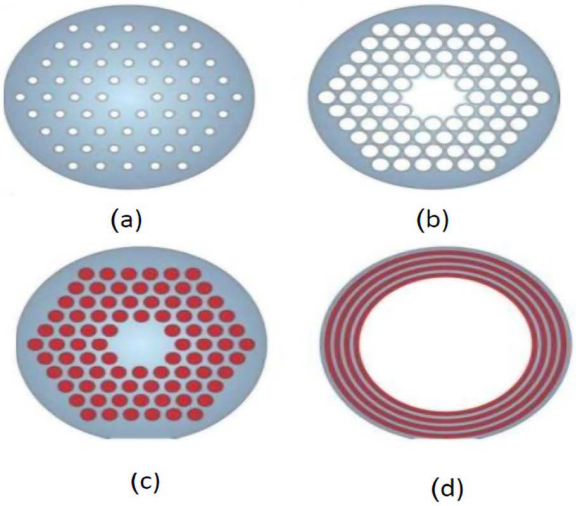

FIGURE 2. Cross-section views of different PFCs designs: (a) fibers with a solid core, (b) fibers with a hollow core, (c) fibers with a solid core and holes filled liquid, and (d) cylindrical hollow multilayer fibers [2].

For sensing applications, the light signal should propagate only through the core and be tightly confined within the core region. Photonic crystal fiber performance evaluation parameters (i.e., evaluation metrics) are primarily relative sensitivity (*RS*), confinement loss (*CL*), effective area (A_{eff}), effective material loss (*EML*), birefringence (*B*), and numerical aperture (*NA*).

The confinement loss property, which is dependent on the imaginary part of the complex effective refractive index, is used to determine the confinement of the light. Equation (3) is used to calculate the confinement loss (*CL*) [63], [64].

$$CL = \frac{4\pi f}{c} * Im\left(n_{eff}\right) \quad \text{cm}^{-1} \tag{3}$$

where the f denotes the operating frequency, c denotes to the speed of light, and Im(n_{eff}) denotes the imaginary value of the effective refractive index.

Effective material loss is the amount of light absorbed per unit length by the background material (EML). The loss of material molecules could cause it as a result of heat generated by enhanced light-matter interaction. The *EML* will be negligible if the PCF model is designed correctly and the background region is reduced. Equation (4) was utilized to derive this vital parameter for the PCF based on perturbation theory [63]–[65].

$$EML = \left(\frac{\sqrt{\frac{\varepsilon_0}{\mu_0}} \int_{mat} n_{mat} \left|E\right|^2 \alpha_{mat} dA}{\int_{all} 0.5^* \left(E^* H\right) \hat{z} dA} \right) \quad \text{cm}^{-1} \tag{4}$$

where H indicates the strength of the magnetic field, E indicates the electric field strength, and ε_0 and μ_0 denote the permittivity and permeability of free space, respectively. n_{mat} is the material's refractive index in the background, and α_{mat} indicates the bulk substance's absorption loss.

The Effective area (A_{eff}), also known as the light-transmitting region, is another significant characteristic. The electric field distribution (E) should be included within the core for the fundamental mode to propagate. The effective area of any PCF-based sensor analyses its actual detecting zone. This characteristic indicates the nature of any fiber's optical nonlinearities and a PCF's effective mode area. Equation (5) is used to calculate the effective area [63], [64].

$$A_{eff} = \frac{\left(\iint \left|E\right|^2 dxdy\right)^2}{\left(\iint \left|E\right|^4 dxdy\right)} \quad \mu\text{m}^2 \tag{5}$$

The numerical aperture (*NA*) value indicates the range of incident light angles that fiber receives and transmits. It is a unitless property dictated by the speed of light (c) and the frequency of operation (f). For sensing applications, a higher *NA* is preferred, which is achieved by lowering the effective area. Equation (6) is used to determine the numerical aperture value [63], [66].

$$NA = \frac{1}{\sqrt{1 + \frac{\pi f^2 (A_{eff})}{c^2}}} \tag{6}$$

Birefringence (B) measures the amount of irregularity among the air holes of the core and cladding region. The parameter indicates the polarization maintaining capability of a PCF. Birefringence is a phenomenon where incident light is divided into two components. When the transmitted light is observed through the optically anisotropic sample, two components of light with a different phase are detected. This phase difference is the main parameter of the birefringence. The phase difference depends on the angle of incidence and the incident polarization direction [67]. By breaking the PCF's geometrical symmetry, high birefringence can be obtained. Its numerical value is determined by the difference in refractive index between the $n_{eff}{}^x$ and $n_{eff}{}^y$. Equation (7) is used to calculate the Birefringence.

$$B = \left| n_{eff}{}^x - n_{eff}{}^y \right| \tag{7}$$

where $n_{eff}{}^x$ and $n_{eff}{}^y$ represent the effective refractive index of x and y modes, respectively [66].

The relative sensitivity (*RS*) of any PCF-based sensor is the essential optical feature that directly computes its sensing capability. The power percentage parameter, It quantifies the amount of light power contained within the core in relation to the total injected power, is directly related to the relative sensitivity parameter. Equation (8) is used to calculate the relative sensitivity [64], [66].

$$RS = \left(\left(\frac{\int\limits_{sample} \mathrm{Re}\left(E_x H_y - E_y H_x\right) dxdy}{\int\limits_{all} \mathrm{Re}\left(E_x H_y - E_y H_x\right) dxdy} \right) * \frac{n_a}{n_{eff}} \right) * 100\% \tag{8}$$

where n_a denotes the refractive index of the analyte and n_{eff} represents the real section of the effective refractive index. While *Ex, Ey* indicates the electric field in x and y polarization, respectively, and *Hx, Hy* indicates the magnetic field in x and y polarization, respectively.

Figure 3 illustrates performance evaluation parameters (i.e., evaluation metrics) for each type of photonic crystal.

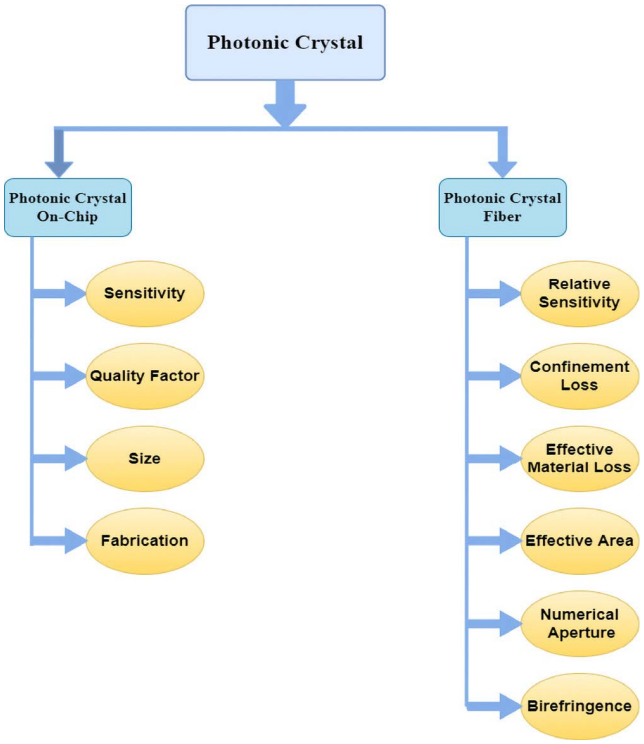

FIGURE 3. The evaluation metrics for each type of photonic crystal.

Surface plasmon resonance (SPR) technology is an optical phenomenon that occurs when electrons energized by polarised light waves oscillate within the metal-dielectric contact. When the core guided mode is combined with the surface plasmon mode, an SPR sensor achieves resonance. SPR has garnered considerable interest due to its real-time capability and high sensitivity. Recently, the PCF has shown promise advantage in SPR excitation due to the fact that phase synchronization between the core guided and plasmonic modes may be accomplished by inserting air holes into the optical fiber to reduce the average refractive index of the fiber [68], [69].

However, there are several significant issues with the PCF-based SPR sensors. The primary issue is the difficulties of fabrication of the PCF-based SPR sensors. It is challenging to coat the inside surface of microstructure optical fibers with silver or gold layers. The sensor quality is dependent on the fabrication method, which means that immature technologies may result in a significant coupling loss for the PCF-SPR sensor. Another major drawback of the PCF-SPR sensor is the uniformity of the metal coating either on the outside or inside of the fiber. Until now, both physical and chemical approaches have been used to coat metal layers onto fibers. However, none of them can ensure the uniformity of the metal layer on a curved surface [70]. Gold or silver are the most frequently used plasmonic metals. While gold is more chemically stable and has a higher sensitivity, the existence of band to band transitions and surface roughness are all drawbacks of gold-coated SPR sensors. Silver has a more defined resonance peak, indicating greater detection accuracy. However, it is susceptible to oxidation, reducing its precision, particularly when sensing aqueous-based analytes [71].

III. ON-CHIP PHOTONIC CRYSTAL BIOMEDICAL SENSORS

A. GLUCOSE SENSOR BASED RING RESONATOR

The first photonic crystal sensor reviewed in this work is utilized to determine glucose, albumin, urea, and bilirubin concentrations in blood and urine [72]. The sensor is constructed in two dimensions using two-dimensional polymer composites using circular rods arranged in a square lattice. PhCs manage the movement of light within the sensor design through defects that can be employed for sensing. It consists of 21 × 21 lattice rods are considered for the design of the biosensor. The lattice constant is defined as a distance between adjacent rods equal to 540 nm, indicated by the letter ''a''. The rod has a radius of 100nm. The inner and outer rods have radiuses of 50 and 100 nanometers, respectively.

Moreover, the rod radius at the low and high ring resonators is 86 nm, giving a more significant output transmission. The Si rod has a refractive index of 3.46 and is surrounded by air. The rod shape is circular, where the Dielectric constant of the Silicon rod is considered to be 11.97, and the sensor entire size is approximately $11.4\mu\mathrm{m} \times 11.4\mu\mathrm{m}$, as shown in Figure 4. The first PBG has a normalized frequency range of (0.435-0.295) a/λ, associated with a wavelength range of (1241-1830) nm. The second PBG is between (0.754-0.732) a/λ, with a wavelength range of (716-737) nm. The first photonic bandgap is chosen for sensor design because it encompasses the second and third windows in optical communication. The recommended sensor is meant to work between the wavelength range (1540-1550) nm.

The described sensor measures the urine glucose concentration ranges of 0.625 to 5 gm/dl. Moreover, the blood glucose concentration is in the range of 180 to 342 gm/dl.

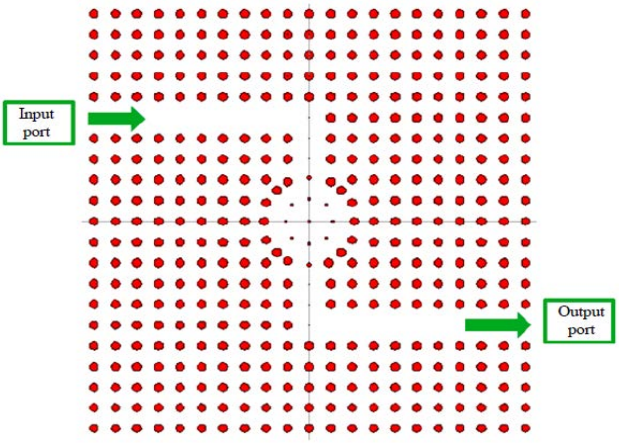

FIGURE 4. Schematic diagram of the glucose sensor [72].

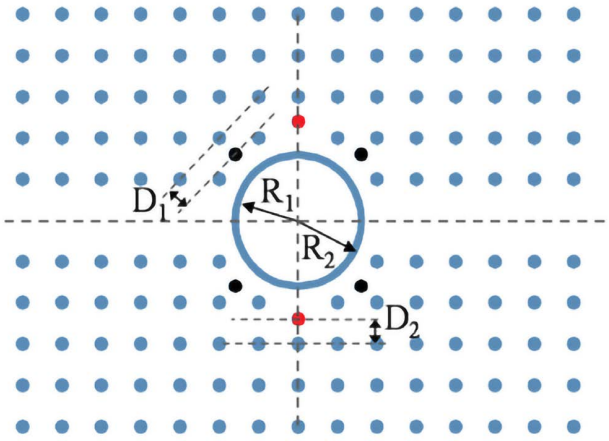

FIGURE 5. The PhC biosensor based on input and output port waveguide and a ring [73].

When the level of glucose in urine and blood rises, so does the refractive index of the urine; nevertheless, the output power of a PhC-based sensor decreases. The presented sensor is based on the principle of decreasing the intensity while raising the refractive index. The sensor's normalized output power and quality factor are listed in Table 1 and Table 2 for urine and blood glucose concentrations. All results are carried at a resonant wavelength of 1585 nm.

TABLE 1. Urine glucose concentration.

Urine glucose concentration	Quality factor	Normalized output power
Normal (0-15mg/dl)	264	1
0.625gm/dl	269	0.96
1.25gm/dl	260	0.92
2.5gm/dl	252	0.85
5gm/dl	217	0.55

TABLE 2. Blood glucose concentration.

Blood glucose concentration	Quality factor	Normalized output power
Normal (165-180mg/dl)	264	1
182 gm/dl	260	0.9
(205-289) gm/dl	252	0.83
342 gm/dl	269	0.75

B. LABEL-FREE BIOMEDICAL SENSOR FOR BASAL CANCER

The second work that will be reviewed in this work is used for the detection of basal cancer. The sensor is produced using a 2D square lattice of GaAs rods. The lattice constant is set to be 410 nm and is denoted by the symbol ''a'', while the radius of the rods is 74.6 nm and is denoted by ''r''. This form of lattice establishes an energy bandgap among T.M. modes. Figure 5 illustrates the suggested PhC sensor in this research. A row of rods is removed to create the incoming and outgoing waveguides. The GaAs ring is positioned in the structure's center, serving as a resonator between the ports of input and output. The radius of the cylindrical ring is 615 nm on the inside and 697 nm on the outside. R_1 is set to be1.5*a, R_2 is set ''t'' be 1.7*a, D_1 is set to be 0.57*a, and finally, D_2 is set to be 0.6*a where ''a'' represents the lattice constant. The remaining rods have a radius of 0.182*a [73]. The cylindrical ring is filled with the analyte material whose refractive index is to be determined. The structure is composed of 2 waveguides and a ring resonator. SiO2 is used to fill the area between the rods. The central ring hollow core is the only unoccupied space. When the analyte is deposited onto the structure, it fills the resonator's internal space.

The sensor presented does not have cavities; meanwhile, it shows an extremely high-quality factor. It exhibits a high level of resistance to fabrication and lithography mistakes. Their final advantage is the simplicity of their design. The result shows that the sensor has a sensitivity of 720 nm/RIU. This is because the resonance is strongly constrained within the ring. It is desirable for the PhC sensor to show sensitivity to changes in the material's refractive index to be sensed while also being insensitive to changes in the rods or holes radius. The biosensor was initially built for the typical 1550 nm wavelength. Meanwhile, just a few nanometer shifts in the operating frequency during production caused the authors to adapt by adjusting the wavelength of the input. To employ such high-Q (narrow-bandwidth) resonators, extremely precise and expensive lithography is necessary. The sensor structures exhibit a reasonably high sensitivity. These sensors are well suited for laboratory on-chip applications.

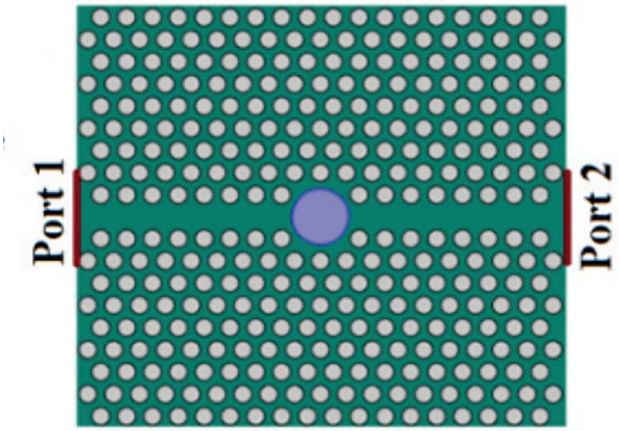

FIGURE 6. Illustrates a cross-section of the 2D PhC biosensor with the central microcavity filled with glucose solution [74].

C. GLUCOSE MONITORING BASED ON ELLIPTICAL MICROCAVITY

The PhC platform that was highlighted in this research includes a GaN dielectric slab with air holes drilled in it and is used for glucose monitoring. As illustrated in Figure 6, the air holes with a radius of r = 0.345a form a hexagonal lattice with a lattice constant of 500 nm. At a wavelength of 1400 nm, The GaN dielectric slab has a dielectric constant of 4.94. GaN is used in a wide variety of devices, such as LEDs and solar cells. Due to its low-temperature deposition, it possesses exceptionally high crystalline quality. Additionally, GaN is insoluble in water and can be used in various high-temperature applications such as optoelectronics. Due to the significant index contrast between GaN (dielectric permittivity of 4.94) and air, GaN is also an excellent option for photonic crystal applications. As a result, sufficient confinement between the defective channel and the analyte-filled core cavity can be obtained, resulting in extremely high sensitivity. The photonic bandgap in this design can vary from 1200 nm to 1850 nm [74]. The biosensor is created by eliminating the two-dimensional middle horizontal row of air holes. Additionally, In the center of the primary channel defect, a rod with radius R microcavity is placed. The central cavity is supplied by a quantity of glucose solution with a refractive index of ''n'', where n denotes the refractive index of the glucose solution. Equation (9) is used to calculate the refractive index of the glucose solution.

$$n = 0.00011889^{*}C + 1.33230545 \tag{9}$$

where ''C'' denotes the glucose concentration in (g/L), the effect of the microcavity radius R on sensitivity is investigated to improve the biosensor's sensitivity. To feed the proposed structure from port 1, a Gaussian pulse with a width of 0.4 μm and a central carrier wavelength of 1.4 μm was used in this research. The transmission of the moving electromagnetic wave is affected by changes in glucose concentration.

Furthermore, to improve the suggested sensor's sensitivity and transmission, the neighboring holes all-around core microcavity are filled with glucose solution, as seen in Figure 7. Additionally, from a practical standpoint, it is critical to maintaining a minimum gap of 15 nm among the borders of the core microcavity and the surrounding holes filled with glucose solution. This separation value is the optimum upper limit. The radius of the center microcavity R is then estimated using values of 3*r, 3.1*r, and 3.2*r. The results show that the resonance wavelength shift becomes higher than it was in the previous design. Additionally, when the radius of the central microcavity in this structure increases, the sensitivity improves. The sensitivities of the biosensors are 280 nm/RIU, 301.3 nm/RIU, and 330.3 nm/RIU, respectively, associated with R = 3*r, 3.1*r, and 3.2*r.

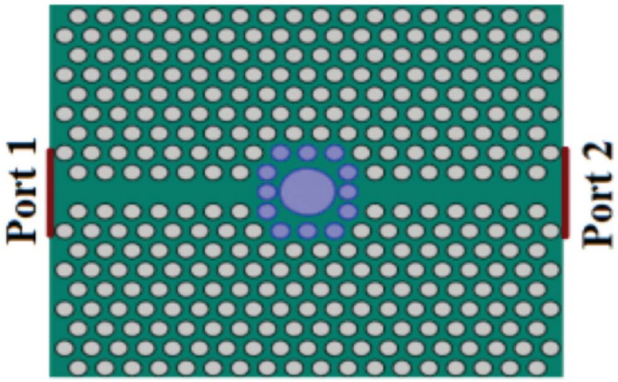

FIGURE 7. The modified 2D PhC biosensor with large central microcavity encircled by 12 holes filled with glucose solution [74].

Furthermore, to improve the sensitivity of more and more of the modified biosensor, The ellipticity of the central microcavity is illustrated, which is surrounded by holes filled with glucose solution. In this modification, the effect of the primary diameter is modified from 2.2*a to 2.6*a. On the other hand, the minor diameter, on the other hand, is kept at 2.2a for practical reasons in order to keep a minimum gap of 15 nm between the borders of surrounding holes filled with glucose solution and the center microcavity, as illustrated in Figure. 8, The sensitivity changes when the primary diameter of the elliptical microcavity is changed. At the central radius of 2.6*a, the proposed 2D PhC has a sensitivity of 422 nm/RIU. The sensor quality factor is also calculated using the resonance wavelength and the output transmission's FWHM. According to the numerical data, the proposed PhC biosensor has a quality factor of 549.2, which is very high as expected.

D. ELLIPTICAL RESONATOR PHOTONIC CRYSTAL FOR BLOOD COMPONENTS DETECTION

The following reviewed work will present a photonic crystal ring resonator-based biosensor design to detect blood components at a wavelength range of (1530-1615) nm. The variations in quality factor, transmission output power, and

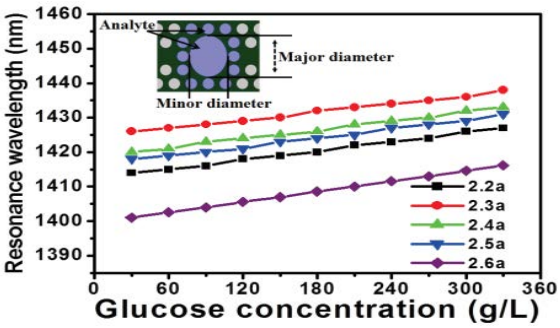

FIGURE 8. The elliptical microcavity's resonance wavelength changes as a function of glucose concentration at various major diameter values [74].

refractive index of blood components such as haemoglobin, white blood components (WBC), red blood components (RBC), blood sugar, and blood urea are sensed. Because each blood component has a different refractive index, the resonance wavelength and output power vary to identify the blood component [75]. The developed PhC-based biosensor is constituted of a cubic array of circular rods positioned upon an air background, as illustrated in Figure 9. The size of the rods is $11.4 \times 9.2\mu m^2$ which contains of 21×17 rods placed as a hexagonal lattice. The rod has a radius of 100nm, whereas the spacing between the adjacent two rods is 540nm, also known as the lattice constant "a". The circular silicon rod has a refractive index of 3.46. The elliptical resonator of the design is located in the core of the structure, and the front and back radius of the circular rod are both 100 nm. The sensor contains input and output ports utilized to transmit optical signals of varying wavelengths.

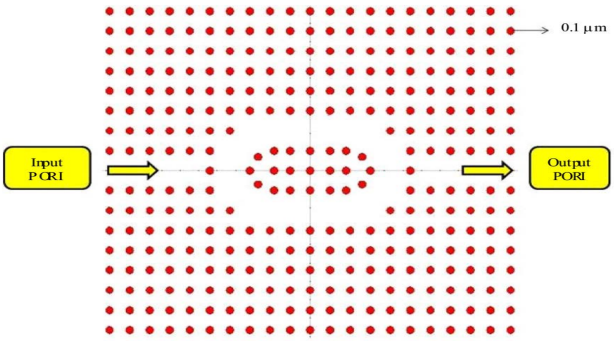

FIGURE 9. The proposed biosensor includes an elliptical ring resonator [75].

The band diagram depicts a PBG with two operating at wavelengths of (1200-1800) nm and (748-814) nm, respectively. The PBG, with a wavelength range of (1200-1800) nm, is suitable for the third optical window in this system. When the light wave enters the waveguide and moves through the elliptical structure of the resonator, The output signal's power is determined using a power monitor located at the output port. The acquired output response is then evaluated to identify the resonance wavelength of 1590 nm, and the output power is 100% with no losses. Finally, a value of 257.5 is established for the Quality factor.

E. HOLLOW-CORE PHOTONIC CRYSTAL FOR CANCER DETECTION

This section will summarize a novel technique for sensing many cells, both normal or malignant, using a two-dimensional photonic crystal waveguide (PCW). The structure shown here comprises five rods made of silicon imprinted on a square lattice with a middle hole and background of air. The study explored two different types of living cells: the normal cell (INOK) and the malignant cell (YD-10B). The primary purpose of using this structure is to use the defect area's enhanced light-guiding characteristics [76]. The defect is formed into the PhC structure by removing the core rod, which causes the electric field to be confined inside the defect area, shown in Figure 10. Structure elements such as lattice constant, circular rod diameter, and background material refractive index are perfectly chosen for the reliable detection of cancerous cells. The suggested square lattice structure has a dimension of $5 \times 5\ \mu m^2$, with a lattice constant of 1000 nm, the rods have a diameter of 450 nm, and a rod height of 500 nm silicon based. The wavelength of the light is chosen to be 650 nm.

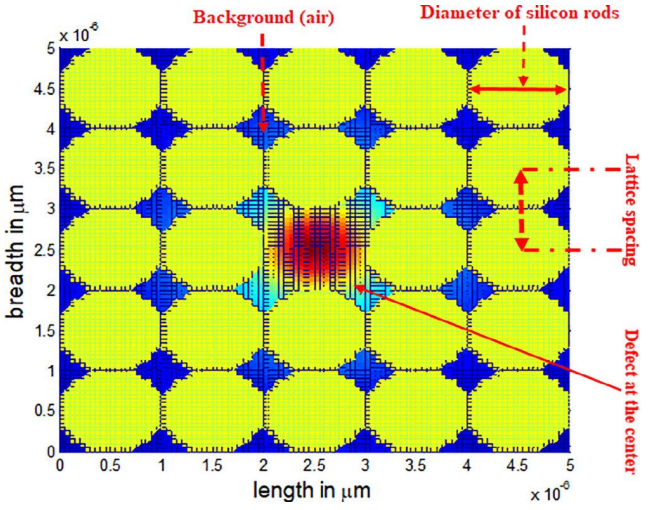

FIGURE 10. Shows a cross-sectional of the designed PCW with a central defect [76].

The sensor results indicated that normal cells reflect wavelengths between (604-623 nm), but malignant cells reflect wavelengths between (565-579 nm). Additionally, the transmitted output power is evaluated, claiming that the proposed design radiates a significantly higher power for malignant cells. Finally, it is shown that the sensor exhibits a maximum sensitivity of 2360.12 nm/RIU, a resolution of $1.78^{*}10^{-6}$, and a very high-quality factor of 99.765, all of which support the sensor's efficiency. As a result of the sensing principles outlined above, the presented structure may be an excellent option for bio-photonics applications.

F. DOUBLE HOLE MICROCAVITY PHOTONIC CRYSTAL FOR MALARIA DETECTION

The next work that is highlighted presents a 2D photonic crystal biomedical sensor with a double hole cavity based on the refractive index; the sensor is designed, simulated, and evaluated. The research objective is to present high sensitivity for diagnosing malaria at its most influential stage. The design requires complex production techniques to fabricate. It has a very high-quality factor, excellent sensitivity, and smaller size of 9.4 × 5.5 μm^2 [77]. The suggested sensor construction for detecting malaria stages is represented in Figure 11. The proposed design consists of silicon rods in a two-dimensional hexagonal lattice with a refractive index of 3.42 on a background of air with a refraction index of 1. The lattice constant "a" is equal to 0.8μm, which represents the distance between adjacent rods. The radius of silicon rods "r" is equal to 0.240μm. The dimensions of the proposed structure are 9.4 × 5.5 μm^2. Three bandgaps are present in the structure. The main band has a range wavelength of (3.523-2.536) μm, the second band has a wavelength range of (1.909-1.491) μm, and the third band has a range wavelength of (1.255-1.067) μm. The input wavelength of 1550 nm is used to guarantee that all optical signal processing devices and networks are compatible.

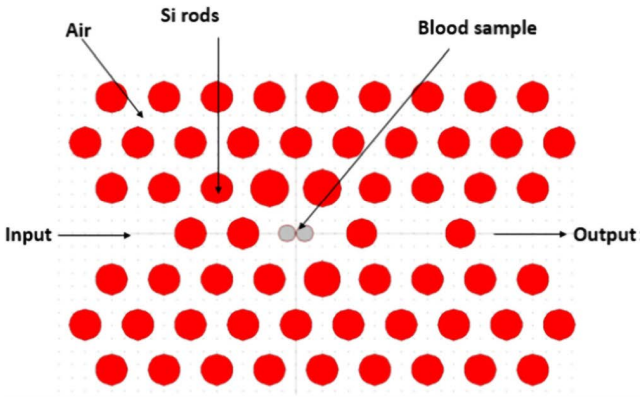

FIGURE 11. The proposed design with double hole cavity defect [77].

The presented design demonstrates that an acceptable sensitivity is obtained while providing an ultra high-quality factor and compactness. The design sensitivity and quality-factors are as follows, for sensitivity it shows Schizont stage = 427 nm/RIU, Trophozoites stage = 416 nm/RIU, Ring stage = 406 nm/RIU, Normal stage = 401 nm/RIU. The quality factor shows that Schizont stage = 5974.80, Trophozoites stage = 5390, Ring stage = 5978, Normal stage = 7187. The proposed sensor provides an ultra-quality factor with very acceptable sensitivity with fabrication possibility.

G. MICROCAVITY PHOTONIC CRYSTAL FOR PANCREATIC CANCER DETECTION

In this work, Plasma samples from patients with pancreatic cancer contained three plasma proteins are demonstrated experimentally using a 2D on-chip photonic crystal sensor and compare the detection sensitivity of the enzyme-linked immunosorbent assay to that of a traditional immunoassay utilizing an enzyme-linked immunosorbent assay (ELISA). Higher sensitivity is attained, which allows for early detection of the plasma proteins and results in a decreased sample volume requirement. The sensor detected proteins HGF and MIP in pancreatic cancer patient plasma at concentrations of 9.813 pg/mL and 15.437 pg/mL, respectively. Two PhC microcavities models were introduced, with identical sluggish light effects and high-quality factor but distinct analyte fill fractions. Using a 193 nm U.V. photolithography production approach, the biosensor was identified in various dilutions of patient plasma samples down to 50 times their original concentration. All devices were manufactured using a commercially available standard CMOS foundry, demonstrating the capability for high volume fabrication [78].

The proposed two models of the sensor are shown in Figure 12, using scanning electron microscopy (SEM) of the L13 PhC microcavity sensor with and without nanoholes. The sensor was produced in Epixfab, Ghent, Belgium, using photolithography followed by reactive ion etching. The microcavities are created in silicon at a wavelength of 220 nm on a silicon-on-insulator wafer using a PhC composed of a triangle lattice that contains air holes with R=112.5 nm hole radius. The nanoholes have a radius of $R_{.D.} = 0.4*R$ and are positioned in the lattice, as shown in Figure 12. Sharp resonances with a quality factor of 22,000 and 12,000 are obtained with and without nanoholes in the L13 PC microcavities, respectively. In addition, sensitivity for L13 is 68 nm/RIU and 112 nm/RIU for L13 with nanoholes.

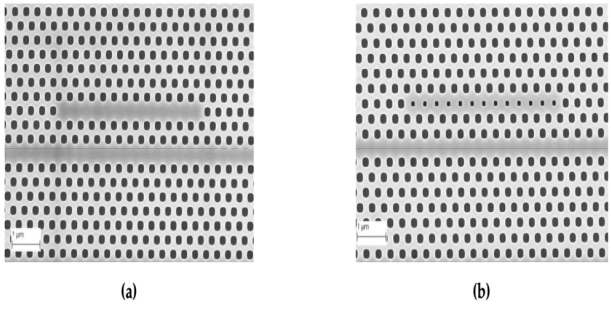

FIGURE 12. Images from SEM (a) L13 PhC microcavity and (b) L13 PC microcavity with nanoholes [78].

To prove that the sensor presented can detect various biomarkers associated with pancreatic cancer, biosensing was used to evaluate HGF, MIP, and Fasligand, which were previously detected using ELISA However, they were present in larger concentrations in ELISA. The same proteins were found in the tests after a 10-times dilution of the input material. MIP has a 0.08 nm resonance wavelength shift, while HGF has a 0.1 nm resonance wavelength shift. Fasligand demonstrated a resonance wavelength shift of 0.04 nm. This relates to the OSA limit of detection.

TABLE 3. Comparisons between ON-CHIP Photonic Crystal biosensors literatures.

Ref	Lattice type	Detection target	Operating technique	Operating wavelength (nm)	Size (μm^2)	Sensitivity (nm/RIU)	Quality Factor	Detection limit	Package used	Fabrication / Simulation
[72] 2017	Square	Glucose in Urine and Blood	Ring resonator	1585	11.4 ×11.4	NA	269	0.001	Rsoft	Simulation
[73] 2018	Square	Basal Cancer	Circular ring resonator	1550	NA	720	NA	NA	Rsoft	Simulation
[74] 2015	Triangular	Glucose Monitoring	Elliptical microcavity	1400-1430	NA	422	549.2	NA	NA	Simulation
[75] 2019	Square	Blood Components	Elliptical ring resonator	1590	11.4×9.2	-	257.5	NA	Rsoft	Simulation
[76] 2020	Square	Cancer	Hollow core	650	5×5	2360	99.76	$1.78*10^{-6}$	NA	Simulation
[77] 2020	Triangular	Malaria	Double hole microcavity	1550	9.4×5.5	427	7187.2	NA	Rsoft	Simulation
[78] 2020	Triangular	Pancreatic Cancer	L13 Microcavities	1536	NA	112	22,000	0.04 nm	NA	Fabrication

Table 3 represents a comparison between literatures that are summarized through section III. Square lattice on-chip Phc based cancer sensor provides the optimum sensitivity of 2360 nm/RIU with a noticeable detection limit of $1.78*10^{-6}$ in [76]. This may be on the price of quality factor performance and not matching the commercial operating window (i.e., 1550 nm). When viewing the size (i.e., in μm^2- mainly size by rods is huge) as a key evaluation metric, especially for on-chip Phc based designs, ref [76] provides novel compactness (i.e., $5 \times 5\ \mu m^2$). Finally, on-chip pancreatic cancer sensor that is presented in [78] provides the optimal possible quality factor with a value of 22,000 associated with a fabrication ability. This is done with a relatively low sensitivity performance and an absence of data related to the fabrication size.

IV. PHOTONIC CRYSTAL FIBER BIOMEDICAL SENSORS

A. HOLLOW-CORE PCF

The first reviewed paper in PCF represents a photonic crystal fiber (PCF) based on a hollow-core optical waveguide that is presented and studied for its potential to rapidly identify many types of malignant cells found in the human body. The refractive indices of normal and malignant cells differ, and these differences are used to evaluate the other significant optical properties. The physical construction of the sensor is exceptionally uncomplicated, letting it be easily manufactured using present manufacturing methods [79]. A two-dimensional representation of the proposed cancer cell sensor, complete with all structural characteristics, is shown in Figure 13. TOPAS, and Zenox are the most used background materials for terahertz based PCFs because of their exceptional properties and reduced absorption losses in comparison to other optical glasses. The proposed sensor's

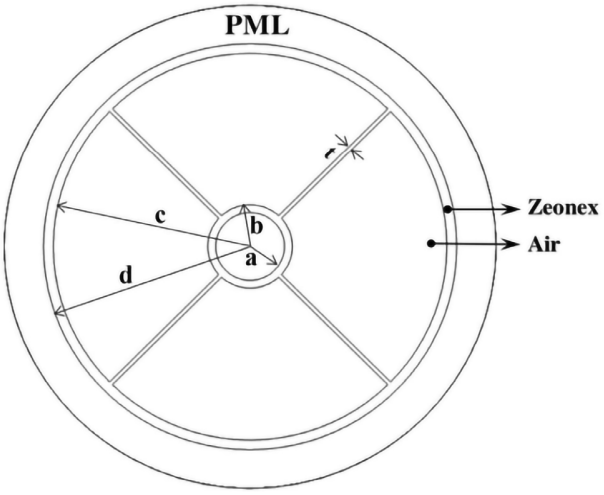

FIGURE 13. A two-dimensional representation of the proposed malignant cells detector [79].

background material is Zeonex, with maximum optical visibility and negligible absorption loss.

The core is constructed with a single circular air hole of radius "r" into which normal or malignant cell samples will be injected. Four-quarter circular-type air holes are inserted in the cladding portion, with the internal and exterior radius marked by "b" and "c," respectively. The "t" indicates the strut's thickness between two air holes. Finally, the cladding section's exterior border is determined by a circle with radius "d". All geometric properties are related to c, where a=0.2*c, b=0.215*c, and t=0.0215*c, and "d" is 5% larger than "c". A circular PML boundary condition is used at the sensor's outermost region; its principal function is to absorb

the light signal entering the core and moving toward the cladding, so avoiding reflection back into the core.

All the simulation studies are done within a frequency of 2.5 THz. The relative sensitivity of a sensor should be as high as possible in order to be considered reasonable; in this design, it has a relative sensitivity of about 98 %. Loss, which comes in two kinds for PCF-based sensors: *EML* and confinement loss, is another essential metric. The first is created by energy absorption in the background substance, while the cladding air holes induce the other one. When the geometric parameters are appropriately set, this sensor provides extremely low confinement loss (about 10^{-8}dB/m) and negligible *EML* 5.5×10^{-3}cm^{-1} for malignant cells. The supplied fiber has an *NA* of roughly 0.43 at 2.5 THz under optimal geometric conditions, which improves the characteristics of the fiber.

Finally, the proposed cancer cell detector's effective area was investigated under various conditions. Because light becomes increasingly restricted at higher operating frequencies, the effective area diminishes as the operating frequency rises. The A_{eff} of the PCF-based detector at 2.5 THz and under optimal conditions is 2.1×10^{-8} m^2, which is extraordinarily low, allowing for increasing interaction of light and analyte.

B. COMPACT CLADDING PCF

This review offers a unique design of the PCF, a hexagonal crystalline core surrounded by a compact hexagonal cladding used in a packed photonic crystal fiber (CC-PCF)-based optical sensor for sensing RBCs, hemoglobin, WBCs, plasma, and water. The presented sensor consists of two regions they are the core and cladding regions. The core is hexagonally packed and contains circular air holes of the same dimension. The core consists of seven non-overlapping rings. In addition, each circle features seven circular air holes, six of which surround one central air hole. Each circle also has seven circular air holes, six of which surround one central air hole. The core region's air holes have the same pattern and size, making manufacturing more manageable. Considering a diverse range of sensing analytes in the core region, including RBCs, hemoglobin, WBCs, plasma, and water [80].

Also, the cladding is organized the same as the core structure. Each circular air hole in the cladding section can be combined with its six adjacent air holes to make a circle. The air holes in the cladding are uniform in diameter of $d_{cl} = 330.45\mu$m. The distance between the centers of two air cavities is referred to as pitch (Λ). The cladding section maintains an air filling fraction of 0.92, which provides more excellent fiber manufacturing flexibility. Additionally, the core has circular holes with $d_{co} = 45.25\ \mu$m and $\Lambda_{co} = 48.95\ \mu$m, which provides flexibility in design. A circular PML has been employed to absorb incident radiation without reflection around the fiber cladding. In this structure, the background material was selected to be TOPAS, as shown in Figure 14.

The presented biosensor CC-PCF was studied for a broad THz range ranging from 1.5 to 3.5 THz, and it was

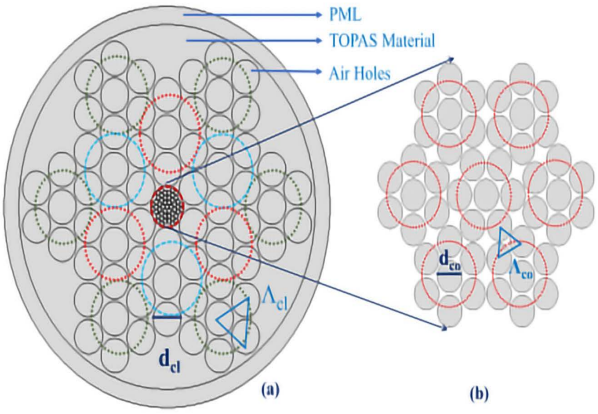

FIGURE 14. A 2D view of the planned sensor's cladding region (b) Zooming view of the core's interior portion [80].

objective of delivering outstanding relative sensitivity and reduced confinement loss. At 1.5 THz frequency, an outstanding relative sensitivity response of 80.9% for RBC, 80.5% for hemoglobin, 80.1% for WBC, 79.9% for plasma, and 79.3% for water are obtained. At the same THz frequency, a confinement loss of 1.23×10^{-11}dB/m for RBC, 8.36×10^{-12} for hemoglobin, 4.39×10^{-12} dB/m for WBC, 2.39×10^{-12} dB/m for plasma, and 1.31×10^{-12} dB/m for water were obtained. Additionally, the realized effective area range for the various blood components is $1.55 \times 10^5 \mu$m^2 at 1.5 THz operating frequency.

C. DECAGONAL SOLID CORE PCF

The following work highlights a description of a decagonal photonic crystal fiber with tremendous sensitivity and negligible confinement loss for detecting blood elements. Blood components like plasma, glucose, RBC, and WBC are used to fill the core. Because liquid may easily infiltrate the core pores, the solid core surrounded by a ring of air holes provides an advantage for detecting biomedical analytes. TOPAS is the material to be utilized as the PCF's background. A Perfectly Matched Layer is utilized as a boundary condition in the cladding's outer layer. The sensor is intended to work at the THz frequency range. Figure 15 depicts a cross-sectional view of the presented PCF sensor. The four decagonal circular air hole rings of the cladding zone enhance the passage of polarised light into the core region. The solid core is built up of rings of air holes that can be invaded by detecting analytes to boost sensing performance. This leads to a growth of the effective area, which results in higher sensitivity [81].

The air holes in the given design have a radius of R=40μm and a diameter of d=2R=80μm in both the core and cladding. The exact diameter of the air holes in the core and cladding will simplify the manufacturing. The distance between the centers of two holes is referred to as pitch and equals 86 μm. The layers in the cladding region are separated by 248μm. The core radius is considered to be $R_{Core} = 178\mu$m, the large core radius enhancing the light's

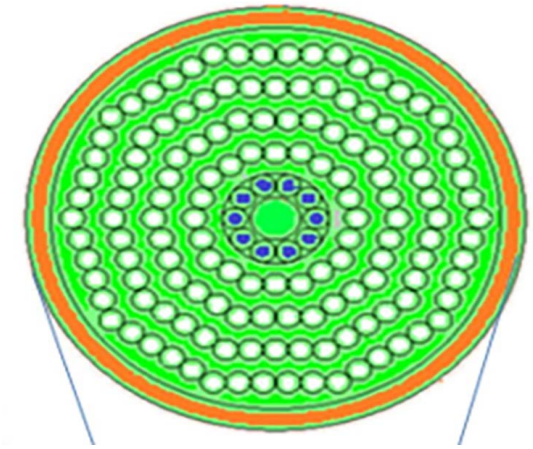

FIGURE 15. A cross-sectional view of proposed PCF [81].

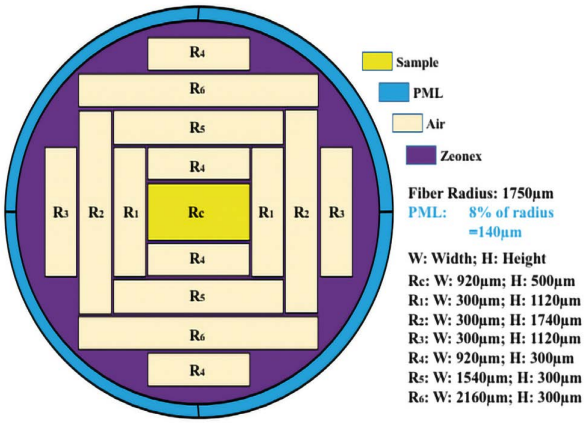

FIGURE 16. Optimal MRC-PCF model cross-sectional view [82].

confinement in the core, and the sensor ring width is assumed to be 98 μm. A PML serves as a restriction boundary for radiation absorption on the PCF sensor's outer surface. The background material is TOPAS for this PCF rather than silica because of its superior optical transparency. The relative sensitivity of a sensor is proportional to its fractional power. As the fractional power density in the core increase, the higher the sensitivity is increased. The sensitivity of the glucose, plasma, WBC, and RBC at a frequency of 1 THz have a value of 84.55%, 85.09%, 85.62%, and 87.68%, respectively. The sensor has shallow confinement loss values for glucose, plasma, WBC, and RBC, which are 7.92×10^{-09} dB/m, 6.66×10^{-9} dB/m, 3.14×10^{-9} dB/m, and 1.86×10^{-9} dB/m, respectively.

The highest effective area determined through simulation is 1.86×10^5 μm^2. The core area of the design structure is around 1.04×10^5 μm^2, approximately 56% of the effective area. It implies that the best factors of design were used to create the specified sensor structure. The designed PCF structure exhibits controlled birefringence across the entire frequency range. At 1 THz, the RBC has the lowest birefringence of 5.1×10^{-5} because their refractive index is the highest, and glucose is the largest birefringence of 1×10^{-4} because their refractive index is the lowest of all blood components.

D. MONO RECTANGULAR CORE PCF FOR SKIN AND BLOOD CANCER

In this review, a unique approach for accurately detecting cancer cells in the blood and skin utilizing a PCF-based sensor. The suggested sensor has an asymmetrical configuration of rectangular holes, with a single rectangle as the core region. The optimal mono-rectangular core (MRC-PCF) is presented in Figure 16. The proposed MRC-PCF has a total radius of 1750 μm and is accompanied on the inner side by a perfectly matched layer (PML) with an 8% radius thickness. PML acts as an anti-reflection layer, preventing signals from being reflected back into the fiber. The core section is defined by a single rectangle, R_c. The core's height and width are 500 and 920 μm, respectively. In the cladding zone, fourteen rectangular air holes are positioned asymmetrically. The cladding has six distinct rectangle designs designated by the letters R_1 through R_6. The width (W) and height (H) values for each rectangle are shown in Figure 16. The pitch of the presented structure is 310 μm, and the strut, or the distance between two successive rectangles, is kept at 10 μm. Zeonex is used to supplement the indicated MRC-PCF. The primary advantage of Zeonex is its constant refractive index in the THz range. Additionally, Zeonex inherits a high level of chemical resistance, glass transmigration heat, and humidity sensitivity. The authors chose hollow-core PCF over porous PCF because it has a higher surface area and can accommodate many analytes [82].

The sensor is made specifically for the detection of jurkat and basal cells. The simulation result indicates this model's increased performance in diagnosing malignant cells. The presented sensor achieves 96.74% sensitivity at 2.0 THz. The maximum confinement loss at 2.0 THz observed for this sensor is only 2.41×10^{-14} cm^{-1}. However, the *EML* remains at 0.01131. Furthermore, building the core and cladding region with only rectangular-shaped holes simplifies manufacturing using current production procedures. The optimal MRC model has a relatively high area for all analytes due to the large area in the core region. For different target samples, the value of the effective area ranges from 2.606×10^{-7} to 2.684×10^{-7} m^2 at a frequency of 2.0 THz. The birefringence for the optimal MRC shows a nearly similar value for 0.0006 for all analytes at 2.0 THz.

E. TRICORE PCF FOR GLUCOSE DETECTION

The following review discusses the use of a tri-core photonic crystal fiber to calculate the increased compact sensitivities of a glucose sensor in the existence of human blood analytically. One hollow channel filled with analyte serves as the liquid core, while the other two hollow channels serve as the silica substrate. This structure is unique in that it is constructed entirely of a single material. It is capable of tuning its sensitivity to detect the presence of glucose in human blood

at deficient levels (g/l) using a minor variation in glucose content (g/l) [83]. The tricore PCF glucose sensor uses a triangular lattice configuration with three regional ring air holes, as shown in Figure 17. The middle air hole serves as the analyte core in the construction of a tricore PCF. Simultaneously, the second-row middle circular is filled with silica background material and serves as a silica core. The proposed PCF sensor's dimensions have been carefully chosen to give exceptional sensitivity over a broad spectral range. The pitch constant of uniformly spaced air holes is set at $\Lambda = 2.3$ μm. When filled with the analyte, the center core's diameter (d_2) is chosen to be 0.9 μm. To achieve the birefringence effect, the diameter (d) surrounding the air pores on both sides of the silica core is slightly increased from the d_1 value and assigned to 2.2 μm. Adjust the remaining cladding holes to $d_1 = 1.4$ μm. The outer shell is 120 μm in circumference. To attain increased sensitivity, the giving structural dimensions are significantly increased. The dimensions d and d_2 were given further consideration because they had a more significant effect on sensitive results. The background material of the fiber is fused silica, and the R.I. of the sample glucose concentration is determined using (9).

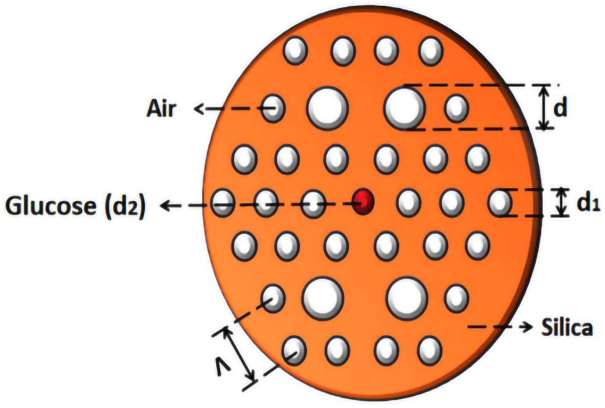

FIGURE 17. Cross-sectional view of the proposed PCF sensor [83].

The novel tricore PCF glucose sensor is designed to attain the best possible sensitivity. The primary goal of these structural topologies is to create the maximum amount of coupling and decoupling, complicated manipulation of light guiding abilities, and switching polarization. The sensitivity for the equivalent wavelength shift detected the slightest fluctuation in glucose concentration between (10-20) g/l. The transmission spectrum demonstrates a maximum wavelength shift of 470 nm for x-polarization and 440 nm for y-polarization in response to the refractive index of glucose, resulting in an increased average sensitivity of 23,267.33 nm/RIU at 470 nm wavelength shift. The suggested structure is completely analyzed and operated using the finite-element method.

F. LIQUID INFILTRATED ELLIPSE PCF BIOSENSOR

This section will summarize a liquid-infiltrated photonic crystal fiber (LI-PCF) for working in THz propagation. Geometric parallelism is accomplished by inserting a massive elliptical at the center filled with liquid cocaine. The suggested sensor's cross-sectional geometry is shown in Figure 18, along with an expanding view of the hollow elliptical core. The core contains a massive elliptical, with parameters a and b denoting the ellipse's main and minor axes, respectively. The principal axis "a" is maintained constant at 370 μm [84]. On the other hand, the "b" axis is adjusted to investigate its effect on the PCF's optical features. The cladding is built with a hexagonal lattice of four and twelve similarly sized circular air holes in the first and second rings. The pitch is defined as a distance between consecutive air holes centers is denoted by the air filling fraction, which is the ratio of the diameter of the air holes to their pitch and is set to 0.97. Zeonex was chosen as the suggested PCF substrate material because it exhibits negligible material dispersion. The PML density is chosen to be 8% of the cladding's diameter.

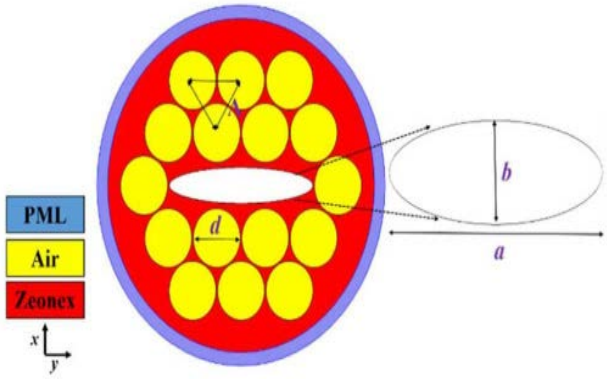

FIGURE 18. The proposed sensor's geometrical spatial extent contains a wide elliptical core range [84].

The ideal design criteria were determined to be 1 THz and b = 95 μm. The suggested PCF has a low confinement loss of 1.95×10^{-3} cm^{-1} and 9.42×10^{-4} cm^{-1}, high relative sensitivity of 87.02% and 85.82%, and an exceptionally small *EML* of 0.009 and 0.012 cm^{-1}, respectively for the x and y polarization modes. Moreover, the fiber has a great birefringence of 1.8×10^{-2} at 1 THz. The suggested design also has a large effective area; at 1 THz operating frequency, the effective areas are 1.11×10^5 and 1.24×10^5 μm^2, respectively, for the x, y polarization modes. On the other hand, the numerical apertures are 0.45 and 0.43 for x and y polarization, respectively. The large core ellipse produces birefringence and improves the sensing of a significant amount of cocaine. The proposed fiber can be mass-produced utilizing the preform casting method.

G. RECTANGLE POROUS CORE PCF BIOSENSOR

The final review presents a rectangle-based porous core photonic crystal fiber (PCF) is built to propagate a THz wave efficiently. The fiber core and cladding are both designed with rectangular air holes. The PCF sensor is shown

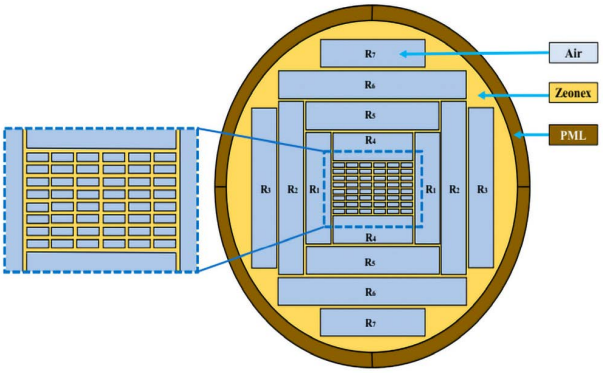

FIGURE 19. The suggested optimum PCF model's cross-section [85].

in Figure 19. The PCF has a radius of 1800 μm, which includes a 140 μm perfectly matched layer. The center section is composed of 48 tiny symmetrical rectangles. A single rectangle's width and height are 144 μm and 53.74 μm, respectively. The cladding section contains fourteen rectangles varying in height and width. The widths of R_1, R_2, and R_3 are all the same (300 μm), and their heights are 1120 μm, 1740 μm, and 1208 μm, respectively. Similarly, the widths of R_4, R_5, R_6, and R_7 are 920 μm, 1540μm, 2160 μm, and 1608 μm, respectively [85]. The proposed PCF model's background material is chosen to be Zeonex, where Zeonex has a tolerated temperature of 138 C°, making it more suitable with other high-temperature polymers. Because of its high molecular weight, it is also better suited for microstructure fiber manufacturing than other current polymers.

Several optical factors have been investigated in order to assess the efficacy of the suggested sensor. This performance assessment is carried out in the THz region, which spans from (0.5-1.5) THz. To achieve the optimal porosity for this model, the authors modified the strut value in the core region, resulting in three alternative porosity values, namely 86% (7.5μm strut), 81% (10μm strut), and 77% (12.5μm strut). The best parameters attributes are found to be at a strut of 10 μm at a frequency of 1.3 THz. The value of the effective area at 1.3 THz is found to be 34×10^4 μm^2, while the value of the *NA* is 0.2179. At 1.3 THz, the *EML* has a value at 86%, 81%, and 77% porosity models are 0.0030, 0.0039, and 0.0045 cm^{-1}, respectively. Moreover, all three models exhibit significantly less confinement loss right after 0.8 THz. At 1.3 THz, the confinement loss values for the 86%, 81%, and 77% porosity models are 0.03×10^{-11}, 1.06×10^{-12}, and 5.96×10^{-13} cm^{-1}, respectively. The optimum model's relative sensitivities in the x and y polarisations at 1.3 THz are found to be 74.55% for x-polarisation and 72.85% for y-polarisation. Rectangles are utilized to model the suggested PCF design, which allows for manufacturing.

Table 4 represents a comparison between PCF-based biosensor literatures that are summarized in section IV. According to operating frequency, all the PCF-based biosensors have acceptable speed with the THz range. Ref [79] provides the optimum operating frequency for cancer sensing. Regarding the design effective area, all literatures that are summarized have an effective design area in the range of 10^{-7} to 10^{-8} m^2. Again, cancer based PCF biosensor [79] provides the optimum effective area of 2.1×10^{-8} m^2. In this point, one can highlight the superiority of on-chip based PhC biosensors compared to PCF based ones regarding compactness. The higher the relative sensitivity, the better the PCF-based sensor. Ref [79], for the 3rd evaluation metric (i.e., relative sensitivity), provide the optimum possible performance with a 98%. To this point, one should indicate that the performance in relative sensitivity shows a slightly larger deviation than that in operating frequency and effective area (i.e., performance not close to each other). The optimum performance for birefringence is provided by blood components PCF-based biomedical sensor [81] with a value of 5.1×10^{-5}. This is associated with acceptable operating frequency, effective area, and relative sensitivity. When viewing the performance of confinement loss and converting values to a unified unit of measurement, the mono rectangular design that is used for skin and blood cancer detection [82] provides the optimum performance with 2.41×10^{-14} cm^{-1}. This design shows high operating frequency, acceptable, effective design area, high relative sensitivity, and acceptable birefringence. The performance of EML shows the convergence of values. The optimum performance can be extracted from [85] with 0.0039 cm^{-1}. Finally, the numerical aperture that should be as high as possible (i.e., for a certain limit to permit only single-mode operation) is found to provide the optimum value of 0.45 in [84]. This may be achieved with a price in operating frequency, birefringence, and confinement loss.

V. NUMERICAL METHODS AND AVAILABLE COMMERCIAL SOFTWARE PACKAGES FOR SIMULATION OF PHOTONIC CRYSTALS

Numerous numerical techniques have emerged as viable alternatives when closed-form solutions encounter obstacles. An intensive effort has been made in the field of optics and photonics-based devices. The solution of Maxwell's equations is critical for the advancement of simulation techniques. They are tasked with obtaining band diagrams, transmission spectra, field patterns, and other associated data for the presented constructions [86]. Computational photonics problems can be classified into three types: frequency domain eigenproblems, frequency domain responses, and time-domain simulations. Another categorization scheme is possible, one that is based on numerical methods and discretization techniques (i.e., into nodes or elements). They will focus on reducing unknowns in order to save time and memory. These include the finite difference time domain method (FDTD), the finite element method (FEM), Plane-Wave Expansion Method (PWEM), the spectral method (S.M.), and the boundary element method (BEM).

There is no perfect technique that solves all problems without introducing complications. As a result, the method will be applied in accordance with the nature of the problem being studied. In Table 5, a brief overview of several numerical

TABLE 4. Comparisons between photonic crystal Fiber biosensors literatures.

Ref	Lattice type	Detection target	Operating frequency	Background Material	Effective area (m^2)	Relative Sensitivity	Birefringence	Confinement loss	EML (cm^{-1})	Numerical Aperture	Package used
[79] 2021	NA	Cancer	2.5 THz	Zeonex	2.1×10^{-8}	98%	NA	10^{-8} dB/m	5.5×10^{-3}	0.43	Comsol
[80] 2019	Hexagonal	Blood Components	1.5 THz	Topas	$1.55\times10^{5}\mu$	80.9%	NA	1.31×10^{-12} dB/m	NA	NA	Comsol
[81] 2021	Decagonal	Blood Components	1 THz	Topas	$1.86\times10^{5}\mu$	87.68%	5.1×10^{-5}	1.86×10^{-9} dB/m	NA	NA	Comsol
[82] 2021	Mono Rectangular	Cancer	2 THz	Zeonex	2.606×10^{-7}	96.74%	0.0006	2.41×10^{-14} cm^{-1}	0.01131	NA	Comsol
[83] 2018	Triangular lattice	Glucose detection	NA	Silica	NA	S=23,267 nm/RIU	NA	NA	NA	NA	Comsol
[84] 2020	Triangular lattice with ellipse	Biosensor	1 THz	Zeonex	$1.24\times10^{5}\mu$	87.02%	1.8×10^{-2}	9.42×10^{-4} cm^{-1}	0.009	0.45	Comsol
[85] 2020	Rectangular porous core	Biosensor	1.3 THz	Zeonex	$3.4\times10^{5}\mu$	74.55%	0.0153	0.03×10^{-11} cm^{-1}	0.0039	0.2179	Comsol

methods applicable to photonic crystal applications will be provided. Numerous samples for various software packages were listed according to the analytical approach utilized.

VI. SOME NOVEL TRENDS OF PHOTONIC CRYSTAL

During this review, several avenues for the continuation of this study became evident. The topics which were considered worthwhile are summarized below:

A. TOPOLOGY PROBLEM

One of the most active study areas is determining the optimal design topology for a photonic crystal as a sensor. This area of research has been explored for decades. The research is still ongoing at this moment because it contains an unlimited number of undiscovered topologies yet. The uniqueness of the optimal topology that covers the required metrics is still so far impossible.

B. STUDYING THE BIOMEDICAL SENSORS PERFORMANCE UNDER DIFFERENT ENVIRONMENTAL CONDITIONS

Earlier papers on PhCs based on dielectric media examined by the researchers assumed that the dielectric properties of the constituent layers were temperature independent and nondispersive. Semiconductor materials are classified as one of the elements of a photonic crystal, considering semiconductors dielectric properties change with temperature. Still studying the performance under different temperature condition, either heating or cooling using closed formulas or COMSOL software, need more investigation.

C. OPTIMIZATION TECHNIQUES FOR SIMULATION AND OPTIMIZATION OF THE PERFORMANCE OF PHOTONIC CRYSTAL BIOSENSORS

One of the most challenging topics is getting the optimum values for design parameters to get the optimal evaluation metrics. For the design of PhCs, the typical trial-and-error technique based on physical perceptions and parametric research has yielded significant results. This procedure, however, is inefficient and time-consuming, and the design approach may also be inefficient. A systematic approach would formulate the problem using proper objective functions and constraints and then solve it using topological optimization techniques [87]. Iterative optimization of topology is a numerical computation-based approach. Numerical approaches such as the finite difference method, the finite element method (FEM), the block-iterative frequency-domain approach, and the plane wave expansion method are frequently used to precisely simulate and optimize photonic crystal structures. These methods, however, are computationally intensive when dealing with complicated photonic crystal structures that must be simulated numerous times to reach an optimum solution. Iterative assessments of this type are also dependent on the quantity of input design parameters that require optimization. Topology optimization developed in structural engineering to distribute parameters within a given domain so that the resulting structure performs optimally or as desired.

Non-gradient topology optimization (NGTO) techniques, such as the genetic algorithm (G.A.), were also extensively employed to optimize the topology of structures. The computational cost of topology optimization is primarily due to the iterative performance examination of structures. NGTO requires many structural trials, and its computing efficiency may be a concern when optimizing topology with a large number of design variables. Numerous researchers have examined approaches for optimizing topology. Significant progress has been made in developing topology optimization methods, laying a foundation for their multidisciplinary and multiphysics applications [87], [88].

D. APPLICATION OF MACHINE LEARNING TECHNIQUES FOR DESIGNING BIOMEDICAL SENSORS

The development of disruptive technologies such as high-speed optical communication and computation,

TABLE 5. Comparison between some numerical methods used in photonic crystal applications [86].

Computational method	Finite Difference Time-Domain method (FDTD)	Plane Wave Expansion Method (PWEM)	Finite Element Method (FEM)
Analysis domain	Time	Frequency	Frequency
Application	1) Calculation of transmission and reflection spectra. 2) Modeling nonlinear devices, transient processes, and extremely massive devices.	1) Determine the Bloch modes and eigenfrequencies of infinite periodic systems.	1) Simple approximations defined on each element using low degree polynomials are used to depict complicated and irregular geometries.
Field Equations	1) Grid-based structure construction (both in time and space). 2) Must observe how the fields evolve and scatter across the grid in order to attain a solution.	1) Expressed mathematically as a superposition of plane waves. 2) The Fourier expansion technique is utilized. 3) The structure must have a finite unit cell. 4) It is classified as a spectral technique.	1) Reduce the structure to a collection of finite elements of varying sizes and shapes (cuboids in 3D-irregular triangles or tetrahedral in 2D)
Advantages	1) Powerful. 2) Flexible. 3) Simple. 4) Easily handle large 3D devices.	1)Simple. 2)Easy determination of band gaps for a given polarisation.	1) Overcome the slow convergence of the (PWEM) 2) Consider material discontinuities in the dielectric structure. 3) Fast, reliable, and very accurate. 4) Preferable for low-frequency problems or high-Quality factor structures.
Disadvantages	1) Expensive in terms of computing. 2) Challenges associated with applying boundary conditions along curved borders. 3) Difficulties in representing complex geometric domains. 4) Long convergence time for low-frequency problems or high-Quality factor structures. 5) Application with dispersive materials is limited.	1) Restricted to modeling structures with an infinite number of periodic elements. 2) Unable to compute transmission and reflection spectra.	1) Results are dependent on the number of elements analyzed. 2) Requires a fast computer. 3) Time consuming. 4) Requires the solution of a complex system of equations at each point of interest in the frequency spectrum.
Software	1) Opti-wave (OptiFDTD) 2) RSoft (FullWAVE) 3) Lumerical (FDTD solutions) 4) CST	1) RSoft (Band solution) 2) Lumerical (Mode solutions)	1) COMSOL Multiphysics 2) FIMMWAVE

ultrasensitive sensor detection and imaging, and quantum information processing has been facilitated by creating novel photonic structures, materials, devices, and systems. For the last two decades, significant progress and success have been achieved with artificially made photonic structures, such as photonic crystals and plasmonic nanostructures, which provide unequaled capabilities for influencing light-matter interactions and enabling novel device concepts [89]. In general, these computational electromagnetics simulations approach the design problem by geographically and temporally discretizing Maxwell's equations, starting with specified initial and boundary conditions. By building sufficient meshes and iteration steps, we may determine exactly the optical properties of a particular structure. Nonetheless, we frequently find ourselves in need of fine-tuning. The geometry and execute simulations for many iterations in order to reach the desired results gradually. Due to simulation power and time limits, this approach heavily relies on prior knowledge of the design templates. In order to find the ideal structure, only a few design parameters are modified. Deep learning enables a computer model comprised of multiple layers of processing units to acquire knowledge about the various levels of abstraction present in the data. Deep learning's distinguishing advantages originate from its data-driven approach, which lets the model discover meaningful information automatically from vast volumes of data, in sharp contrast to physics- or rule-based approaches. Over the last few years, deep learning has emerged as a breakthrough new tool for photonic design.

Deep learning has progressed well beyond its origins as a computational model of biological neural systems. It has evolved into a strong instrument for resolving complicated issues by layering abstractions from massive data. Deep learning and other artificial intelligence approaches are reshaping optical design, integration, and measurement in the photonics community at the moment. Deep learning algorithms have already proved their enormous potential for

optimizing the design, architecture, material selection, and overall performance of photonic structures and optical systems. They will continue to develop fresh techniques for accelerating optical measurements and detecting novel optical events [90]. Machine and deep learning have recently risen to prominence in a variety of fields. Additionally, a geometric deep learning approach has been suggested for studying nanophotonic structures. In 2018, photonic crystal dispersion relations [91] and Q-factors [92] were computed and optimized using extreme learning machines and deep learning. As a result, machine learning (ML) techniques have been advocated recently for computing various optical characteristics of photonic crystals. They integrate finite element simulations and artificial neural networks (ANN) to perform computations quickly and accurately [93].

E. EQUIVALENT CIRCUIT MODELS FOR THE PHOTONIC CRYSTAL BIOSENSORS

Searching for the equivalent circuit models for the photonic crystal biosensors remains a mystery that has been unsolved yet. Our research group is now attempting to develop circuit models based on the PhC sensors measurements, but no significant approach to the model has been introduced so far. The PhC circuit models will provide rapid, simple, and computationally efficient techniques for describing the PhC sensors performance from an engineers perspective. Thus, it may be more advantageous to model the PhCs behavior using an electrical circuit model. Describing a circuit-level implementation of a PhCs, either small-signal or large-signal behavior, is a hot topic that requires deep investigation.

VII. CONCLUSION

This review presents an intensive investigation in the field of PhC-based optical biomedical sensors, emphasizing current advancements produced in the field. The presented studies and their associated findings show that PhC-based structures play an essential role in optical biosensors. Many PhC architectures, sensing qualities, and mechanisms are thoroughly addressed. The sensing process depended heavily on the modification of the optical characteristics of the PhC due to changes in the refractive index or lattice constant. Additionally, the critical technologies for future PhC-based sensors will include controllability, integration, and novel design and methodology explorations, which will open the way to develop exceptionally sensitive and integrated biosensors. Brief elaboration is established, and different remarkable characteristics are investigated.

REFERENCES

[1] A. Govdeli, M. C. Sarihan, U. Karaca, and S. Kocaman, "Integrated optical modulator based on transition between photonic bands," *Sci. Rep.*, vol. 8, no. 1, pp. 1–11, Dec. 2018.
[2] S. Obayya, *Computational Photonics*, 1st ed. Hoboken, NJ, USA: Wiley, 2010.
[3] Y. Zhang, Y. Zhao, T. Zhou, and Q. Wu, "Applications and developments of on-chip biochemical sensors based on optofluidic photonic crystal cavities," *Lab Chip*, vol. 18, no. 1, pp. 57–74, Oct. 2018.
[4] Y. N. Zhang, Y. Zhao, and R. Q. Lv, "A review for optical sensors based on photonic crystal cavities," *Sens. Actuators A, Phys.*, vol. 233, pp. 374–389, Sep. 2015.
[5] M. I. Shehata and N. A. Mohammed, "Design and optimization of novel two inputs optical logic gates (NOT, AND, OR and NOR) based on single commercial TW-SOA operating at 40 Gbit/s," *Opt. Quantum Electron.*, vol. 48, no. 6, pp. 1–16, Jun. 2016.
[6] N. A. Mohammed, "Performance evaluation and enhancement of 2×2 Ti:$LiNbO_3$ Mach Zehnder interferometer switch at 1.3 μm and 1.55 μm," *Open Electr. Electron. Eng. J.*, vol. 6, no. 1, pp. 36–49, Dec. 2012.
[7] N. A. Mohammed, H. S. A. Elnasr, and M. H. Aly, "Analysis and design of an electro-optic 2 × 2 switch using Ti:$KNbO_3$ as a waveguide based on MZI at 1.3 μm," *Opt. Quantum Electron.*, vol. 46, no. 2, pp. 295–304, 2014.
[8] N. A. Mohammed, N. M. Okasha, and M. H. Aly, "A wideband apodized FBG dispersion compensator in long haul WDM systems," *J. Optoelectron. Adv. Mater.*, vol. 18, nos. 5–6, pp. 475–479, 2016.
[9] N. A. Mohammed and H. O. El Serafy, "Ultra-sensitive quasi-distributed temperature sensor based on an apodized fiber Bragg grating," *Appl. Opt.*, vol. 57, no. 2, pp. 273–282, Jan. 2018.
[10] N. A. Mohammed and N. M. Okasha, "Single- and dual-band dispersion compensation unit using apodized chirped fiber Bragg grating," *J. Comput. Electron.*, vol. 17, no. 1, pp. 349–360, Mar. 2018.
[11] N. A. Mohammed, M. R. Abaza, and M. H. Aly, "Improved performance of M-ary PPM in different free-space optical channels due to Reed Solomon code using APD," *Int. J. Sci. Eng. Res.*, vol. 2, no. 4, pp. 2–5, 2011.
[12] A. S. El-Wakeel, N. A. Mohammed, and M. H. Aly, "Free space optical communications system performance under atmospheric scattering and turbulence for 850 and 1550 nm operation," *Appl. Opt.*, vol. 55, no. 26, p. 7276, 2016.
[13] N. A. Mohamed, A. M. Aly, A. K. AboulSeoud, and M. H. Aly, "Indoor wireless optical communication systems: Effect of ambient noise," *Opt. Eng.*, vol. 53, no. 5, May 2014, Art. no. 055109.
[14] N. A. Mohammed and K. A. Badawi, "Design and performance evaluation for a non-line of sight VLC dimmable system based on SC-LPPM," *IEEE Access*, vol. 6, pp. 52393–52405, 2018.
[15] N. A. Mohammed and M. A. Elkarim, "Exploring the effect of diffuse reflection on indoor localization systems based on RSSI-VLC," *Opt. Exp.*, vol. 23, no. 16, p. 20297, 2015.
[16] K. A. Badawi, N. A. Mohammed, and M. H. Aly, "Exploring BER performance of a SC-LPPM based LOS-VLC system with distinctive lighting," *J. Optoelectron. Adv. Mater.*, vol. 20, nos. 5–6, pp. 290–301, 2018.
[17] M. A. Elkarim, N. A. Mohammed, and M. H. Aly, "Exploring the performance of indoor localization systems based on VLC-RSSI, including the effect of NLOS components using two light-emitting diode lighting systems," *Opt. Eng.*, vol. 54, no. 10, Oct. 2015, Art. no. 105110.
[18] N. A. Mohammed, K. A. Badawi, A. A. M. Khalaf, and S. El-Rabaie, "Dimming control schemes combining IEEE 802.15.7 and SC-LPPM modulation schemes with an adaptive M-QAM OFDM for indoor LOS VLC systems," *Opto-Electron. Rev.*, vol. 28, no. 4, pp. 203–212, 2020.
[19] N. A. Mohammed, M. M. Elnabawy, and A. A. M. Khalaf, "PAPR reduction using a combination between precoding and nonlinear companding techniques for ACO-OFDM-based VLC systems," *Opto-Electron. Rev.*, vol. 29, pp. 59–70, Jun. 2021.
[20] Mohammed and H. Mansi, "Performance enhancement and capacity enlargement for a DWDM-PON system utilizing an optimized cross seeding Rayleigh backscattering design," *Appl. Sci.*, vol. 9, no. 21, p. 4520, Oct. 2019.
[21] R. Rajasekar and S. Robinson, "Nano-electric field sensor based on two dimensional photonic crystal resonator," *Opt. Mater.*, vol. 85, pp. 474–482, Nov. 2018.
[22] F. Sun, B. Dong, J. Wei, Y. Ma, H. Tian, and C. Lee, "Demonstration of mid-infrared slow light one-dimensional photonic crystal ring resonator with high-order photonic bandgap," *Opt. Exp.*, vol. 28, no. 21, p. 30736, 2020.
[23] H. Sharifi, S. M. Hamidi, and K. Navi, "All-optical photonic crystal logic gates using nonlinear directional coupler," *Photon. Nanostruct.-Fundam. Appl.*, vol. 27, pp. 55–63, Nov. 2017.
[24] A. Dideban, H. Habibiyan, and H. Ghafoorifard, "Photonic crystal channel drop filter based on ring-shaped defects for DWDM systems," *Phys. E, Low-Dimensional Syst. Nanostruct.*, vol. 87, pp. 77–83, Mar. 2017.
[25] J. Divya, S. Selvendran, and A. Sivanantha Raja, "Two-dimensional photonic crystal ring resonator-based channel drop filter for CWDM application," *Photon. Netw. Commun.*, vol. 35, no. 3, pp. 353–363, Jun. 2018.

[26] M. Li, J. Ling, Y. He, U. A. Javid, S. Xue, and Q. Lin, "Lithium niobate photonic-crystal electro-optic modulator," *Nature Commun.*, vol. 11, no. 1, pp. 1–8, Dec. 2020.

[27] G. Marty, S. Combrié, F. Raineri, and A. De Rossi, "Photonic crystal optical parametric oscillator," *Nature Photon.*, vol. 15, no. 1, pp. 53–58, Jan. 2021.

[28] R. Rajasekar, K. Parameshwari, and S. Robinson, "Nano-optical switch based on photonic crystal ring resonator," *Plasmonics*, vol. 14, no. 6, pp. 1687–1697, Dec. 2019.

[29] T. S. Mostafa, N. A. Mohammed, and E. S. M. El-Rabaie, "Ultra-high bit rate all-optical AND/OR logic gates based on photonic crystal with multi-wavelength simultaneous operation," *J. Mod. Opt.*, vol. 66, no. 9, pp. 1005–1016, 2019.

[30] S. Olyaee, M. Seifouri, A. Mohebzadeh-Bahabady, and M. Sardari, "Realization of all-optical NOT and XOR logic gates based on interference effect with high contrast ratio and ultra-compacted size," *Opt. Quantum Electron.*, vol. 50, no. 11, pp. 1–12, Nov. 2018.

[31] F. Parandin and N. Mahtabi, "Design of an ultra-compact and high-contrast ratio all-optical NOR gate," *Opt. Quantum Electron.*, vol. 53, no. 12, pp. 1–9, Dec. 2021.

[32] M. M. Karkhanehchi, F. Parandin, and A. Zahedi, "Design of an all optical half-adder based on 2D photonic crystals," *Photon. Netw. Commun.*, vol. 33, no. 2, pp. 159–165, Apr. 2017.

[33] Y.-C. Jiang, S.-B. Liu, H.-F. Zhang, and X.-K. Kong, "Realization of all optical half-adder based on self-collimated beams by two-dimensional photonic crystals," *Opt. Commun.*, vol. 348, pp. 90–94, Aug. 2015.

[34] F. Parandin, R. Kamarian, and M. Jomour, "A novel design of all optical half-subtractor using a square lattice photonic crystals," *Opt. Quantum Electron.*, vol. 53, no. 2, pp. 1–10, Feb. 2021.

[35] A. Askarian, G. Akbarizadeh, and M. Fartash, "An all-optical half subtractor using photonic crystal based nonlinear ring resonators," *Optik*, vol. 207, Feb. 2020, Art. no. 164424.

[36] T. S. Mostafa, N. A. Mohammed, and E.-S.-M. El-Rabaie, "Ultracompact ultrafast-switching-speed all-optical 4 × 2 encoder based on photonic crystal," *J. Comput. Electron.*, vol. 18, no. 1, pp. 279–292, Mar. 2019.

[37] M. Danaie and B. Kiani, "Design of a label-free photonic crystal refractive index sensor for biomedical applications," *Photon. Nanostruct.-Fundam. Appl.*, vol. 31, pp. 89–98, Sep. 2018.

[38] B. Troia, A. Paolicelli, F. De Leonardis, and V. M. N. Passaro, "Photonic crystals for optical sensing: A review," in *Advances in Photonic Crystals*. Rijeka, Croatia: InTech, 2013, pp. 242–295.

[39] E. Reyes-Vera, C. M. B. Cordeiro, and P. Torres, "Highly sensitive temperature sensor using a Sagnac loop interferometer based on a side-hole photonic crystal fiber filled with metal," *Appl. Opt.*, vol. 56, no. 2, p. 156, 2017.

[40] J.-X. Li, Z.-R. Tong, L. Jing, W.-H. Zhang, J. Qin, and J.-W. Liu, "Fiber temperature and humidity sensor based on photonic crystal fiber coated with graphene oxide," *Opt. Commun.*, vol. 467, Jul. 2020, Art. no. 125707.

[41] A. K. Goyal and S. Pal, "Design and simulation of high-sensitive gas sensor using a ring-shaped photonic crystal waveguide," *Phys. Scripta*, vol. 90, no. 2, p. 25503, 2015.

[42] M. El Beheiry and O. Levi, "Enhanced sensitivity in optofluidic photonic crystal slab biosensors," in *Proc. Opt. InfoBase Conf. Paper*, 2010, vol. 18, no. 22, pp. 1020–1028.

[43] F.-L. Hsiao and C. Lee, "Computational study of photonic crystals nano-ring resonator for biochemical sensing," *IEEE Sensors J.*, vol. 10, no. 7, pp. 1185–1191, Jul. 2010.

[44] S. M. Lo, S. Hu, G. Gaur, Y. Kostoulas, S. M. Weiss, and P. M. Fauchet, "Photonic crystal microring resonator for label-free biosensing," *Opt. Exp.*, vol. 25, no. 6, pp. 7046–7054, Mar. 2017.

[45] J. N. Dash, R. Jha, J. Villatoro, and S. Dass, "Nano-displacement sensor based on photonic crystal fiber modal interferometer," *Opt. Lett.*, vol. 40, no. 4, p. 467, 2015.

[46] W. Suh, O. Solgaard, and S. Fan, "Displacement sensing using evanescent tunneling between guided resonances in photonic crystal slabs," *J. Appl. Phys.*, vol. 98, no. 3, Aug. 2005, Art. no. 033102.

[47] Y. Liu and H. W. M. Salemink, "Sensitive all-optical channel-drop sensor in photonic crystals," *J. Lightw. Technol.*, vol. 33, no. 17, pp. 3672–3678, Sep. 1, 2015.

[48] F. Bougriou, T. Bouchemat, M. Bouchemat, and N. Paraire, "Optofluidic sensor using two-dimensional photonic crystal waveguides," *Eur. Phys. J. Appl. Phys.*, vol. 62, no. 1, p. 11201, Apr. 2013.

[49] J. Guo, R. A. Norte, and S. Gröblacher, "Integrated optical force sensors using focusing photonic crystal arrays," *Opt. Exp.*, vol. 25, no. 8, p. 9196, 2017.

[50] X. Dong, H. Y. Tam, and P. Shum, "Temperature-insensitive strain sensor with polarization-maintaining photonic crystal fiber based Sagnac interferometer," *Appl. Phys. Lett.*, vol. 90, no. 15, pp. 1–4, 2007.

[51] O. L. J. Pursiainen and J. J. Baumberg, "Compact strain-sensitive flexible photonic crystals for sensors," *Appl. Phys. Lett.*, vol. 87, no. 10, pp. 2003–2006, 2005.

[52] C. Lin, Y. Wang, Y. Huang, C. Liao, Z. Bai, M. Hou, Z. Li, and Y. Wang, "Liquid modified photonic crystal fiber for simultaneous temperature and strain measurement," *Photon. Res.*, vol. 5, no. 2, p. 129, 2017.

[53] H. Chopra, R. S. Kaler, and B. Painam, "Photonic crystal waveguide-based biosensor for detection of diseases," *J. Nanophoton.*, vol. 10, no. 3, Aug. 2016, Art. no. 036011.

[54] Y. Akahane, T. Asano, B.-S. Song, and S. Noda, "High-Q photonic nanocavity in a two-dimensional photonic crystal," *Nature*, vol. 425, no. 6961, pp. 944–947, 2003.

[55] J. Vučković, M. Lončar, H. Mabuchi, and A. Scherer, "Optimization of the Q factor in photonic crystal microcavities," *IEEE J. Quantum Electron.*, vol. 38, no. 7, pp. 850–856, Jul. 2002.

[56] M. Notomi, E. Kuramochi, and H. Taniyama, "Ultrahigh-Q nanocavity with 1D photonic gap," *Opt. Exp.*, vol. 16, no. 15, p. 11095, 2008.

[57] Q. Quan and M. Loncar, "Deterministic design of wavelength scale, ultra-high Q photonic crystal nanobeam cavities," *Opt. Exp.*, vol. 19, no. 19, p. 18529, 2011.

[58] P. B. Deotare, M. W. McCutcheon, I. W. Frank, M. Khan, and M. Lončar, "High quality factor photonic crystal nanobeam cavities," *Appl. Phys. Lett.*, vol. 94, no. 12, pp. 65–68, 2009.

[59] N. A. Mohammed, M. M. Hamed, A. A. M. Khalaf, A. Alsayyari, and S. El-Rabaie, "High-sensitivity ultra-quality factor and remarkable compact blood components biomedical sensor based on nanocavity coupled photonic crystal," *Results Phys.*, vol. 14, Sep. 2019, Art. no. 102478.

[60] V. Kaur and S. Singh, "Extremely sensitive multiple sensing ring PCF sensor for lower indexed chemical detection," *Sens. Bio-Sens. Res.*, vol. 15, pp. 12–16, Sep. 2017.

[61] H. Ademgil, "Highly sensitive octagonal photonic crystal fiber based sensor," *Optik*, vol. 125, no. 20, pp. 6274–6278, 2014.

[62] T. Zhang, Y. Zheng, C. Wang, Z. Mu, Y. Liu, and J. Lin, "A review of photonic crystal fiber sensor applications for different physical quantities," *Appl. Spectrosc. Rev.*, vol. 53, no. 6, pp. 486–502, Jul. 2018.

[63] R. H. Jibon, M. Ahmed, and M. K. Hasan, "Identification of detrimental chemicals of plastic products using PCF in the THz regime," *Meas., Sensors*, vol. 17, Oct. 2021, Art. no. 100056.

[64] A. A.-M. Bulbul, R. H. Jibon, S. Biswas, S. T. Pasha, and M. A. Sayeed, "Photonic crystal fiber-based blood components detection in THz regime: Design and simulation," *Sensors Int.*, vol. 2, Dec. 2021, Art. no. 100081.

[65] M. S. Islam, S. Rana, M. R. Islam, M. Faisal, H. Rahman, and J. Sultana, "Porous core photonic crystal fibre for ultra-low material loss in THz regime," *IET Commun.*, vol. 10, no. 16, pp. 2179–2183, Nov. 2016.

[66] M. S. Islam, J. Sultana, K. Ahmed, M. R. Islam, A. Dinovitser, B. W.-H. Ng, and D. Abbott, "A novel approach for spectroscopic chemical identification using photonic crystal fiber in the terahertz regime," *IEEE Sensors J.*, vol. 18, no. 2, pp. 575–582, Jan. 2018.

[67] J. Carriere, R. Narayan, W.-H. Yeh, C. Peng, P. Khulbe, L. Li, R. Anderson, J. Choi, and M. Mansuripur, "2—Principles of optical disk data storage," in *Progess in Optics*, vol. 41, E. Wolf, Ed. Amsterdam, The Netherlands: Elsevier, 2000, pp. 97–179.

[68] C. Liu, W. Su, F. Wang, X. Li, Q. Liu, H. Mu, T. Sun, P. K. Chu, and B. Liu, "Birefringent PCF-based SPR sensor for a broad range of low refractive index detection," *IEEE Photon. Technol. Lett.*, vol. 30, no. 16, pp. 1471–1474, Aug. 15, 2018.

[69] M. S. Islam, J. Sultana, A. Dinovitser, B. W.-H. Ng, and D. Abbott, "A gold coated plasmonic sensor for biomedical and biochemical analyte detection," in *Proc. 43rd Int. Conf. Infr., Millim., Terahertz Waves (IRMMW-THz)*, Sep. 2018, pp. 2–4.

[70] Y. Zhao, Z.-Q. Deng, and J. Li, "Photonic crystal fiber based surface plasmon resonance chemical sensors," *Sens. Actuators B, Chem.*, vol. 202, pp. 557–567, Oct. 2014.

[71] J. N. Dash and R. Jha, "Highly sensitive d shaped PCF sensor based on SPR for near IR," *Opt. Quantum Electron.*, vol. 48, no. 2, pp. 1–7, Feb. 2016.

[72] S. Robinson and N. Dhanlaksmi, "Photonic crystal based biosensor for the detection of glucose concentration in urine," *Photon. Sensors*, vol. 7, no. 1, pp. 11–19, Mar. 2017.

[73] M. Danaie and B. Kiani, "Design of a label-free photonic crystal refractive index sensor for biomedical applications," *Photon. Nanostruct.-Fundam. Appl.*, vol. 31, pp. 89–98, Sep. 2018.
[74] M. S. Mohamed, M. F. O. Hameed, N. F. F. Areed, M. M. El-Okr, and S. S. A. Obayya, "Analysis of highly sensitive photonic crystal biosensor for glucose monitoring," *Appl. Comput. Electromagn. Soc. J.*, vol. 31, no. 7, pp. 836–842, 2016.
[75] R. Arunkumar, T. Suaganya, and S. Robinson, "Design and analysis of 2D photonic crystal based biosensor to detect different blood components," *Photon. Sensors*, vol. 9, no. 1, pp. 69–77, Mar. 2019.
[76] A. Panda and P. P. Devi, "Photonic crystal biosensor for refractive index based cancerous cell detection," *Opt. Fiber Technol.*, vol. 54, Jan. 2020, Art. no. 102123.
[77] N. A. Mohammed, M. M. Hamed, A. A. M. Khalaf, and S. El-Rabaie, "Malaria biosensors with ultra-sensitivity and quality factor based on cavity photonic crystal designs," *Eur. Phys. J. Plus*, vol. 135, no. 11, p. 933, Nov. 2020.
[78] C.-J. Yang, H. Yan, N. Tang, Y. Zou, Y. Al-Hadeethi, X. Xu, H. Dalir, and R. T. Chen, "Ultra sensitivity silicon-based photonic crystal microcavity biosensors for plasma protein detection in patients with pancreatic cancer," *Micromachines*, vol. 11, no. 3, p. 282, Mar. 2020.
[79] A. Habib, A. N. Z. Rashed, H. M. El-Hageen, and A. M. Alatwi, "Extremely sensitive photonic crystal fiber–based cancer cell detector in the terahertz regime," *Plasmonics*, vol. 16, no. 4, pp. 1297–1306, Aug. 2021.
[80] K. Ahmed, F. Ahmed, S. Roy, B. K. Paul, M. N. Aktar, D. Vigneswaran, and M. S. Islam, "Refractive index-based blood components sensing in terahertz spectrum," *IEEE Sensors J.*, vol. 19, no. 9, pp. 3368–3375, May 2019.
[81] A. Kumar, P. Verma, and P. Jindal, "Decagonal solid core PCF based refractive index sensor for blood cells detection in terahertz regime," *Opt. Quantum Electron.*, vol. 53, no. 4, pp. 1–13, Apr. 2021.
[82] M. M. A. Eid, A. N. Z. Rashed, A. A.-M. Bulbul, and E. Podder, "Mono-rectangular core photonic crystal fiber (MRC-PCF) for skin and blood cancer detection," *Plasmonics*, vol. 16, no. 3, pp. 717–727, Jun. 2021.
[83] A. Natesan, K. P. Govindasamy, T. R. Gopal, V. Dhasarathan, and A. H. Aly, "Tricore photonic crystal fibre based refractive index sensor for glucose detection," *IET Optoelectron.*, vol. 13, no. 3, pp. 118–123, Jun. 2019.
[84] N. A. N. B. Suhaimi, I. K. Yakasai, E. Abas, S. Kaijage, and F. Begum, "Modelling and simulation of novel liquid-infiltrated PCF biosensor in terahertz frequencies," *IET Optoelectron.*, vol. 14, no. 6, pp. 411–416, Dec. 2020.
[85] A. A.-M. Bulbul, F. Imam, M. A. Awal, and M. A. P. Mahmud, "A novel ultra-low loss rectangle-based porous-core PCF for efficient THz waveguidance: Design and numerical analysis," *Sensors*, vol. 20, no. 22, p. 6500, Nov. 2020.
[86] T. Mostafa and E.-S. El-Rabaie, "Literature review on all-optical photonic crystal encoders and some novel trends," *Menoufia J. Electron. Eng. Res.*, vol. 28, no. 2, pp. 153–184, Jul. 2019.
[87] W. Li, F. Meng, Y. Chen, Y. F. Li, and X. Huang, "Topology optimization of photonic and phononic crystals and metamaterials: A review," *Adv. Theory Simulations*, vol. 2, no. 7, pp. 1–22, 2019.
[88] H.-W. Dong, Y.-S. Wang, T.-X. Ma, and X.-X. Su, "Topology optimization of simultaneous photonic and phononic bandgaps and highly effective phoxonic cavity," *J. Opt. Soc. Amer. B, Opt. Phys.*, vol. 31, no. 12, p. 2946, 2014.
[89] S. Chugh, A. Gulistan, S. Ghosh, and B. M. A. Rahman, "Machine learning approach for computing optical properties of a photonic crystal fiber," *Opt. Exp.*, vol. 27, no. 25, p. 36414, 2019.
[90] T. Asano and S. Noda, "Optimization of photonic crystal nanocavities based on deep learning," *Opt. Exp.*, vol. 26, no. 25, p. 32704, 2018.
[91] A. S. Ferreira, G. N. Malheiros, and H. E. Hernández, "Computing optical properties of photonic crystals by using multilayer perceptron and extreme learning machine," *J. Lightw. Technol.*, vol. 36, no. 18, pp. 4066–4073, Sep. 15, 2018.
[92] T. Asano and S. Noda, "Optimization of photonic crystal nanocavities based on deep learning," *Opt. Exp.*, vol. 26, no. 25, pp. 32704–32717, 2018.
[93] W. Ma, Z. Liu, Z. A. Kudyshev, A. Boltasseva, W. Cai, and Y. Liu, "Deep learning for the design of photonic structures," *Nature Photon.*, vol. 15, no. 2, pp. 77–90, Feb. 2021.

NAZMI A. MOHAMMED received the Ph.D. degree in wireless optical communications from Alexandria University, Egypt, in 2010. He is currently an Associate Professor at the Electrical Engineering Department, College of Engineering, Shaqra University, Dawadmi, Saudi Arabia. His current research interests include optical communications, optoelectronics, and nano-photonics.

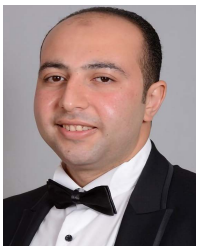

OMAR E. KHEDR was born in Alexandria, Egypt. He received the B.S. degree in electronics and communication engineering from the Alexandria Higher Institute of Engineering and Technology (AIET), Alexandria, in 2009, and the M.S. degree in electrical engineering from the Arab Academy for Science and Technology, Alexandria, in 2015, where he is currently pursuing the Ph.D. degree in electrical engineering. He is also a Teaching Assistant with the Department of Electronics and Communication Engineering, AIET. His research interests include nanotechnology, photonics, optoelectronics, and photonic crystals.

EL-SAYED M. EL-RABAIE was born in Sires Elian, Egypt, in 1953. He received the B.Sc. degree (Hons.) in radio communications from Tanta University, Tanta, Egypt, in 1976, the M.Sc. degree in communication systems from Menoufia University, Menouf, Egypt, in 1981, and the Ph.D. degree in microwave device engineering from the Queen's University of Belfast, Belfast, U.K., in 1986. In his Ph.D. research, he constructed a computer-aided design (CAD) package used in nonlinear circuit simulations based on the harmonic balance techniques. Up to February 1989, he was a Postdoctoral Fellow with the Department of Electronic Engineering, Queen's University of Belfast. He was invited as a Research Fellow with the College of Engineering and Technology, Northern Arizona University, Flagstaff, in 1992, and as a Visiting Professor at the Ecole Polytechnique de Montreal, Montreal, QC, Canada, in 1994. He was the Head of the Electronics and Communication Engineering Department, Faculty of Electronic Engineering, Menoufia University, then the Vice Dean of Postgraduate Studies and Research with the Faculty of Electronic Engineering. He is involved now in different research areas, including CAD of nonlinear microwave circuits, nanotechnology, digital communication systems, and digital image processing. He has authored or coauthored more than 400 articles and 21 textbooks. He was awarded several awards (Salah Amer Award of Electronics in 1993, the Best Researcher on (CAD) from Menoufia University in 1995, and the Best Paper Award on the 2019 36th National Radio Science Conference, NRSC 2019). He acts as a reviewer and a member of the editorial board for several scientific journals. He has shared in translating the First Part of the Arabic Encyclopedia. He is a Reviewer of *Quality Assurance and Accreditation of Egyptian Higher Education* and a member of the Scientific Committee for the Promotion of Professors and Assistant Professors (2019–2022).

ASHRAF A. M. KHALAF received the B.Sc. and M.Sc. degrees in electrical engineering from Minia University, Egypt, in 1989 and 1994, respectively, and the Ph.D. degree in electrical engineering from the Graduate School of Natural Science and Technology, Kanazawa University, Japan, in March 2000. He currently works as a Professor and the Head of the Electronics and Communications Engineering Department, Minia University.